

# A modeling framework for resolving non-linear infrared absorption in an FTIR cell

Master's thesis in Innovative and Sustainable Chemical Engineering

AXEL OLSSON



MASTER'S THESIS 2015

**A modeling framework for  
resolving non-linear infrared  
absorption in an FTIR cell**

AXEL OLSSON



**CHALMERS**  
UNIVERSITY OF TECHNOLOGY

Department of Chemistry and Chemical Engineering  
CHALMERS UNIVERSITY OF TECHNOLOGY  
Gothenburg, Sweden 2015

A modeling framework for  
resolving non-linear infrared  
absorption in an FTIR cell  
AXEL OLSSON

© AXEL OLSSON, 2015.

Supervisor: SOHEIL SOLTANI, Chalmers University of Technology  
Examiner: RONNIE ANDERSSON, Chalmers University of Technology

Master's Thesis 2015  
Department of Chemistry and Chemical Engineering  
Chalmers University of Technology  
SE-412 96 Gothenburg  
Telephone +46 31 772 1000

Cover: Block diagram of compartment model superposed on concentration contour  
plot from CFD analysis.

Typeset in L<sup>A</sup>T<sub>E</sub>X  
Gothenburg, Sweden 2015

A modeling framework for resolving non-linear infrared absorption in an FTIR cell

AXEL OLSSON

Department of Chemistry and Chemical Engineering

Chalmers University of Technology

## Abstract

The need to extract kinetic information from reaction systems in order to determine kinetic parameters is of high importance within chemical engineering and other research fields. The information relies on measured data using infrared absorption technique. As a consequence the quality of the kinetic information is directly linked to the quality of the experimental data. Recent studies to determine the quality has shown that there is a systematic error that arises when compounds that exhibits non-linear relationship between infrared absorption and concentration are measured in transient experiments. This error arises from the infrared analyzer itself and is compensated by the development of a compartment model that works as a corrective algorithm. The compartment model is developed to be of low computational cost in order to resolve transient kinetics by non-linear regression analysis, while still accurately resemble a much more complex computation fluid dynamic model that lay as basis for the compartment model. The models were then compared to evaluate the quality of the developed compartment model by changing the operating conditions of concentrations, flow-rates and signal profile. The high correlation coefficient for the final compartment model  $R^2 = 0.99945$  shows great potential for the model to predict the segregation inside the FTIR cell. The computational time was reduced from approximately 96 hours to 0.05 seconds for a simulated 11 seconds sequence.

Keywords: FTIR, Non-linear absorption, Regression analysis, Compartment model, CSTR, Residence time distribution



## Acknowledgements

After many years as a student, the final piece of the puzzle has been written at the Department of Chemistry and Chemical Engineering at Chalmers University of Technology. Throughout the time I spent thinking, calculating, simulating and writing, all the people surrounding me has been supportive and I want to take the chance to personally extend my gratitude to:

My supervisor **Soheil Soltani** for providing the opportunity to take part of the interesting research he is conducting at the department and as a great support for all my questions and reasoning.

My examiner **Assoc Prof. Ronnie Andersson** for the opportunity to join the research team and providing feedback and new ideas to encourage progress of my work.

Extended gratitude to **Prof. Bengt Andersson** for valuable input and ideas that has been important for my work.

I would also like to send my gratitude to **Per Hultberg, Helena Wennebrink and Mats Karlsson** for being outstanding teachers and giving me a solid academic start.

Finally I want to thank my family immensely, **Lisbeth, Gerth and Annika** that throughout these years as a student always has been supportive, Thank you!

Axel Olsson, Gothenburg, November 2015



## List of abbreviations

BVP – Boundary value problem

CFD – Computational fluid dynamics

COV – Covariance

CSTR - Continuous stirred tank reactor

DOF - Degrees of freedom

FTIR - Fourier transform infrared gas analyzer

IVP - Initial-value problem

IR – Infrared

MUSCL - Monotonic upstream-centered scheme for conservation laws

ODE - Order differential equation

PFR - Plug flow reactor

PPB – Parts per billion

PPM – Parts per million

RAD – Radians

RTD - Residence time distribution

SISO - Single input single output

SSE - Sum of square error

VAR – Variance



# Contents

<b>1</b>	<b>Introduction</b>	<b>1</b>
1.1	Background . . . . .	1
1.2	Problem description . . . . .	3
1.3	Thesis outline . . . . .	4
<b>2</b>	<b>Theory</b>	<b>5</b>
2.1	Infrared absorbance . . . . .	5
2.1.1	Fourier transform infrared gas analyser . . . . .	6
2.2	Computational fluid dynamics . . . . .	6
2.3	Fluid mechanics . . . . .	8
2.3.1	Mean and variance of residence time distribution . . . . .	9
2.3.2	Stagnant zones . . . . .	10
2.3.3	Bypass . . . . .	11
2.3.4	Signal conversion . . . . .	11
2.4	Ideal vessels . . . . .	12
2.4.1	Mathematical formulation . . . . .	13
<b>3</b>	<b>Methods</b>	<b>15</b>
3.1	Compartment modeling . . . . .	15
3.1.1	Degrees of freedom . . . . .	16
3.1.2	Model condition . . . . .	17
3.1.3	Tanks in series . . . . .	17
3.2	Regression analysis . . . . .	19
3.2.1	Non-linear regression . . . . .	20
3.2.2	Parametrization . . . . .	21
3.2.3	Model structure . . . . .	22
3.2.4	Constrained optimization . . . . .	23
3.2.5	ODE Solver . . . . .	24
3.2.6	Script algorithm . . . . .	24
3.3	Resolving internal flow structure . . . . .	25
3.3.1	Structural design . . . . .	25
3.4	Virtual FTIR . . . . .	28
<b>4</b>	<b>Results</b>	<b>31</b>
4.1	Final compartment model . . . . .	31
4.2	Goodness of fit . . . . .	32

4.2.1	Correlation matrix . . . . .	32
4.2.2	Correlation coefficient . . . . .	34
4.3	Concentration . . . . .	35
4.4	Variance . . . . .	36
4.5	Sinusoidal signal . . . . .	36
4.6	Variable flow-rates . . . . .	37
4.7	FTIR comparison . . . . .	38
4.8	Computational time . . . . .	39
<b>5</b>	<b>Conclusion</b>	<b>41</b>
<b>6</b>	<b>References</b>	<b>43</b>
<b>A</b>	<b>Appendix 1</b>	<b>45</b>
A.1	Investigation of time invariance in CFD model . . . . .	45

# 1

## Introduction

Research on reactive systems in chemical engineering are dependent on reliable information about reactions, therefore the need to fully understand the kinetics is of high importance in order to make predictions. To fully understand the reactions it is important to identify the mechanisms, pathways and individual step or steps that may be rate determined. This information is important for processes that are unsteady or as at the Competence Centre for Catalysis at Chalmers University of technology, certain surface reactions in heterogeneous catalysis.

### 1.1 Background

In order to reveal this underlying information about the reactions from experiments, the data from the reactions have to be collected and analyzed in their transient period. Analyzing the reaction data from steady-state experiments this information would be hidden due to that the individual reaction-steps involved would have adjusted to each other. In the transient period of the experiment these mechanisms has not yet adjusted into a state of equilibrium and the information about individual steps, mechanisms and proposed pathways can therefore be collected [1]. The information about the reactions are derived from kinetic analysis which is based on a kinetic model with proposed reaction mechanisms and reaction parameters. This model is then fitted to results from experimental data from the reaction in the transient period. The model and its parameters will then be changed and updated by regression analysis until a good fit between experimental data and the kinetic model is achieved. And the best fit between the proposed kinetic model and experimental data is the model that contains the most accurate information of parameters and reaction-steps. Figure 1.1 below shows the schematic of the procedure on how the parameters for a proposed kinetic model is obtained.

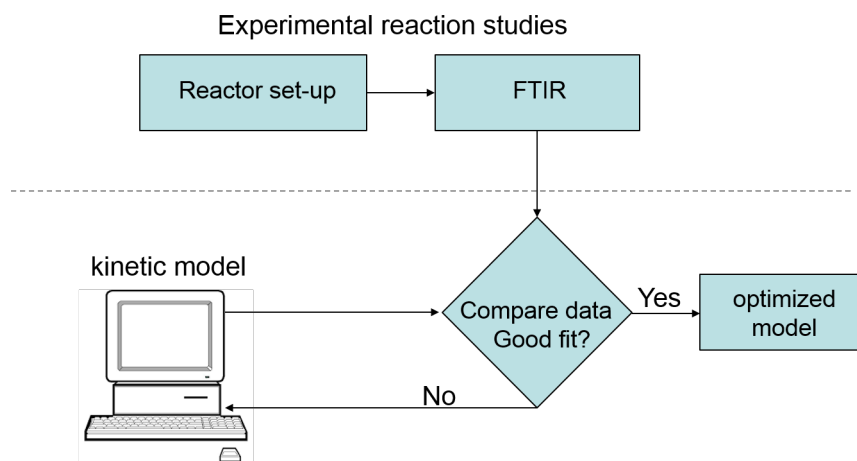


**Figure 1.1:** Schematic layout depicting the procedure used for kinetic modeling.

The experimental data are collected by measuring the products from the reaction of interest in a controlled experimental set-up. A technique available for measuring gaseous product streams from the experimental set-up is the Fourier transform infrared gas analyzer (FTIR) which has a high detection accuracy within the parts per billion, ppb, range for most compounds [10]. By this procedure it is therefore evident that the quality of the kinetic models will rely on the quality of the experimental results. This accuracy has been tested by performing a step-response test over the experimental set-up which therefore can be considered a known input. The difference between this known input and measured output is the time-lag that arises through the system. It was shown that indeed there was a time-lag that arose from the experimental set-up including the FTIR detector. From the step-response test it could be concluded that the actual experimental set-up was of less importance as the major contributor of the total error was found to be in the FTIR itself, 94 % of the total signal distortion [2]. This distortion adheres from hydrodynamic dispersion of the input signal in the detector cell within the FTIR gas analyzer [3]. Signal distortion will mean a loss in temporal resolution which is very important for transient experiments as each individual time step contains valuable information. However this problem has been solved by development of a deconvolution algorithm. The hydrodynamic dispersion adds another problem when the measured compound exhibit a non-linear relationship between concentration and infrared absorption, which is the detection technique used in FTIR. Hydrodynamic dispersion within the cell together with the non-linear absorption cause a systematic error in the transient measurements between detected concentration and actual concentration. Soheil Soltani et al. proved this systematic error by the means of a transient computational fluid dynamic (CFD) simulation of the detector cell with incorporation of infrared absorption. By simulating a step-response with carbon monoxide which is a compound that exhibit the non-linear relationship it was shown that there indeed was a difference between the detected concentration and actual concentration in the detector cell during the transient period [4], which is shown in Figure 1.2 below.

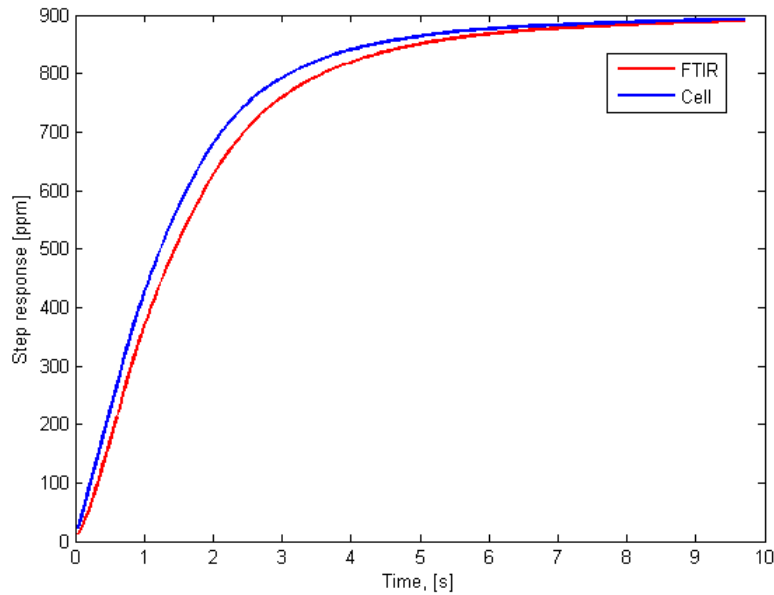


**Figure 1.2:** Systematic error between actual concentration (blue) and detected concentration from infrared absorption (red) for step response 900 ppm CO.

## 1.2 Problem description

The hydrodynamic dispersion together with the non-linear infrared absorption is the source of the systematic error [2]. The error will reduce the quality of the experimental data and have a negative impact on the accuracy of the kinetic models. To increase the quality of the experimental data the systematic error has to be accounted for by a corrective algorithm. The CFD model described above can correct for the systematic error and can therefore be considered as a corrective algorithm. However a major drawback for the CFD model is the need of a known transient input signal to simulate a correct detected result. The solution would be to incorporate the CFD model into the regression analysis of the kinetic model to update the input signal of the CFD model in a iterative procedure to account for the systematic error. The current CFD model takes approximately 96 hours for 10 seconds simulated sequence, which in an iterative procedure will end up using decades of computational time which is unfeasible.

The proposed solution for finding a corrective algorithm is to replace the computational demanding CFD model with a low-cost compartment model that is constructed based on the results from the CFD model. The main focus for the compartment model are that the computational time must be drastically reduced while still producing results that can be comparable to the CFD model.

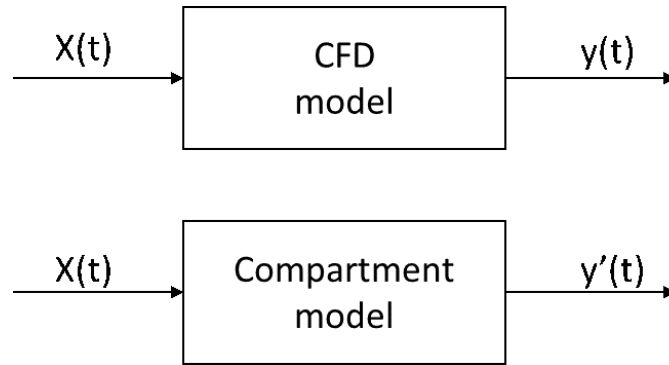


**Figure 1.3:** Schematic block diagram representing the CFD model (top) and compartment model (bottom) with identical input,  $x(t)$ , and corresponding output  $y(t)$  and  $y'(t)$ .

The general aim of the study can be generalized by the block diagram in Figure 1.3 where the error between the two models using identical input should be minimized to assure that the compartment model will predict as similar results as the much more advanced CFD model by minimizing the sum off square error (SSE) for every time-step ( $t$ ).

$$SSE_{min} = (y(t) - y'(t))^2 \quad (1.1)$$

### 1.3 Thesis outline

The thesis will start off with theory to provide information about the FTIR analysis and how the experimental results of ir absorption are put into mathematical formulas that can be used in simulations. This is followed by theory in how the governing mass-balance equation are derived and how they can be connected into a compartment model. Thereafter, theory on how to interpret the concentration output (Residence time distribution, RTD) from the CFD model and transfer the behaviour over to the compartment model. Results from the compartment model will then be compared to a variety of simulated results from the CFD model.

# 2

## Theory

In the framework of the model a variety of physical phenomena has to be incorporated and interconnected. The theory has to be translated into mathematical formulations and the experimental data has to be analysed in order to propose a model that will make accurate predictions.

### 2.1 Infrared absorbance

In order to quantitatively and qualitatively analyze the species of interest in fluids the technique of infrared spectroscopy is applied. This technique identifies the molecule by logging which unique bands of ir-frequency is absorbed by the molecules functional groups [6]. The carbon monoxide is a diatomic molecule with a triplet covalent bond which allow for a distinctive molecular vibration when ir-radiation is absorbed.



For diatomic molecules with covalent bonds there are general principles to calculate the wavenumber using the harmonic oscillator model, which is the ir-frequency the molecule absorbs energy. The wavenumber can be calculated by viewing the molecule as spheres with masses connected with a spring by applying it to Eq. 2.1 to calculate the diatomic wavenumber. For this purpose Argon will act as a perfect solute to CO as the single, non-polarized atom will not absorb any energy which could interfere with the absorbed energy for CO [8].

$$\bar{\nu} = \frac{1}{2\pi c} \sqrt{K \left( \frac{1}{m_1} + \frac{1}{m_2} \right)} \quad (2.1)$$

All data to calculate the wave-number ( $cm^{-1}$ ) are listed in the Table below.

**Table 2.1:** Parameter values to calculate wave-number.

Parameter	Value	Units
K	18	md/Å
c	299 792 458	m/s
$m_1$	12.0107	amu
$m_2$	15.9994	amu

The resulting wavenumber was calculated to  $2110.6 \text{ cm}^{-1}$  which by the experimental result by Jimmy Bak et al. [5] was determined to  $2178.8$  and  $2148.6 \text{ cm}^{-1}$ .

Measurements at different concentration determined that the relationship between detected concentration and absorption is nonlinear and from these data a fifth order polynomial was fitted in order to computationally simulate the correlation between absorbance and concentration [5].

$$C = -0.981 + 8.781A + 0.0554A^2 + 0.00849A^3 - 1.58 \times 10^{-4}A^4 + 7.70 \times 10^5 \quad (2.2)$$

The concentration response ( $C_\lambda$ ) from the FTIR at the CO absorption wavelength ( $\lambda$ ) will be simulated by the known relationship of Beer-Lambert law,  $A_\lambda = \varepsilon_\lambda C s$  [9]. Here the term  $\varepsilon_\lambda$  is the molar absorptivity which is the proportionality constant for the absorption ( $A_\lambda$ ) that is depending on the optical length ( $s$ ) and concentration ( $C_\lambda$ ) in the cell.

$$\varepsilon_\lambda = \frac{A_\lambda}{C s} \quad (2.3)$$

Knowing the concentration range of interest, the experimental nonlinear relationship between absorption, concentration and optical length in the experiment, the molar absorptivity ( $\varepsilon$ ) is computed from a function of concentration ( $y$ ) given by Eq. 2.4 [5].

$$\varepsilon = \frac{-7.864 \times 10^{10} + 0.002278 \times 10^{12}y^2 + 4.497 \times 10^6y + 22.24}{10^{12}y^2 + 333.6 \times 10^6y - 0.5537} \quad (2.4)$$

From this known triplet of molar absorptivity, optical length and actual concentration a representative FTIR response that relies on experimental results can be modeled. This method was implemented by Soltani et al. to show that there will be a systematic error in the FTIR detection during transient experiment [4]. The systematic error from these data was illustrated in Figure 1.2 and adheres from the non-homogeneous concentration that the detector cell will have during a transient measurement.

### 2.1.1 Fourier transform infrared gas analyser

The detector used in the experiments is a *MultiGas 2030* gas analyzer from MKS. At the heart of the analyzer is the detector cell which is the focus for this work and. Inside the heated detector cell the gas emissions from the experimental set-up flows through and absorb energy from the ir-beam which is sent between the end caps 32 times ( $\sim 5$  m optical length) in order to detect the specie concentration throughout the whole cell [10].

## 2.2 Computational fluid dynamics

In order to gain insight of the fluid mechanics inside the detector cell, CFD simulations are highly useful tool to get detailed information which otherwise would be impossible. Previous study of the detector cell made use of a CFD simulation to determine the quality of the FTIR measurements [3]. The simulation were conducted in 3D and based on the internal geometry of the detector cell and the measurements are shown in Figure 2.1.

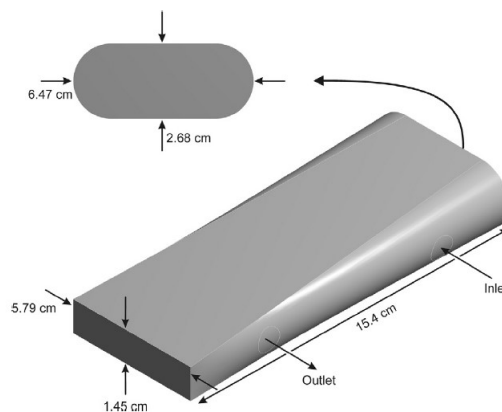


**Figure 2.1:** Detector cell geometry used in CFD simulations.

The CFD model will also be the underlying foundation from which the new simplified model will be compared and assessed on in terms of quality of the predicted results. All the data extracted from the CFD model will be seen as experimental results that the new compartment model should predict. For this reason the quality of the CFD model has to high to assure that the CFD simulation behaves as realistic as possible. The software used for this model is the ANSYS academic package. First of is to assess the flow properties and calculate the Reynold number to verify if the choice to exclude the turbulent flow model and assume that the flow is laminar is correct. The Reynold number calculated at the experimental conditions in the narrowest section in the cell with only argon present. The data used for Eq. 2.5 are are listed in Table 2.2.

$$Re = \frac{\rho D_h v}{\mu} \qquad D_h = \frac{4A}{p} \qquad (2.5)$$

**Table 2.2:** Parameters for calculations.

Parameter	Value	Units	Description
$\rho$	1.05	$kg/m^3$	<i>Density</i> <sup>1</sup>
$D_h$	0.0232	$m$	Hydraulic diameter
$A$	$8.3955 \times 10^{-4}$	$m^2$	Area
$p$	0.1448	[m]	Wetted perimeter
$\mu$	$3.284 \times 10^{-5}$	$kg/(s \times m)$	Viscosity (200°C) <sup>2</sup>
$v$	0.11	$m/s$	Velocity

1)  $PV=nRT$  2)[11]

These conditions results in a Reynold number of 81.7 which is far from the  $\sim 1000$  where the turbulence starts between walls, therefore the laminar condition holds true [12]. Further aspects of the model is the mesh quality, and tests by refine the mesh showed that there were no measurable difference in the result, i.e. the simulated results are not mesh dependent. The total number of cells for this mesh independent solution is approximately. 400000 cells. And the aspect ratio for this mesh shows good quality. The transport equations for this type of laminar flow with

a flow field that is expected to twist and might even swirl should by recommendation be solved by a second order up-wind scheme or MUSCL scheme [13] in order to get transportiveness in the schemes, this was also fulfilled [4]. The simulation is a transient simulation meaning that for each time step the solution must converge. The number of iterations needed for each time step to converge is dependent on how low residual is allowed in the continuity and species transport equations. To maintain high quality a low residual limit is set for the individual equations as shown in Table 2.3.

**Table 2.3:** Residual limits for CFD simulation.

Parameter	Value
Continuity	$10^{-4}$
momentum	$10^{-4}$
Specie	$10^{-4}$

Initially the number of iterations to converge a solution for the initial time steps might reach approximately 500-600 iterations with a time step of 0.05 seconds. As the simulation flow time increases the iterations is reduced to around 200 before the solution converges. To reduce the iterations further the time step needs to be smaller, this would decrease the computational time for each time step but on the other hand increase the number of time steps in the simulation. Still, the quality check shows that the CFD model are of high quality and can be used as a reliable source of data.

## 2.3 Fluid mechanics

In order to properly design the compartment model the characterization of how the concentration profile develops inside the FTIR detector cell is the most important information to be able to enhance the quality of the model [7,14,15].

From fluid mechanics the technique of tracer technology is used to determine flow behavior and to analyze how the concentration profile develops inside the vessel. The concentration profile (RTD) can be determined by running a stable rate of solute trough the vessel, and add a known concentration of tracer with similar properties at the inlet. By measuring the concentration of tracer at the outlet as a function of time, the results will determine how the flow acts inside the vessel [7]. In the experiment Argon is used as the carrier gas due to its inert properties to other gases, and as the tracer CO is used as it is the gas of interest in the experiment. By measuring the time from which the tracer was added at the inlet and then measuring the concentration of the tracer at the outlet the result can be presented as a RTD. There are of course a number of ways to add the tracer that all gives their characteristic response. Most common is the pulse and step response which also will be used in this study to evaluate the hydrodynamic dispersion and convective flow pattern occurring in the cell. Below in Figure 2.2 are illustrations of the pulse and

step-response which will be used. Later, the periodic signal will be used to test and evaluate the compartment model [7].

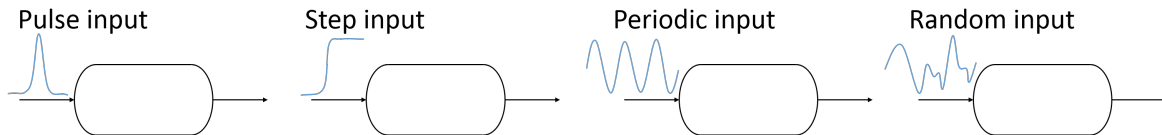


**Figure 2.2:** Different tracer injection methods.

The pulse input can be described as a very quick burst of tracer into the inlet at the start of the experiment. The step response on the other hand has a continuous supply of tracer at a constant rate throughout the whole length of the experiment. From this known input, the output signal will be interpreted on how distorted it is coming out. In fairly ideal conditions the outlet signal will usually be a stretched version of the inlet tracer signal. The outlet response of the known inlet tracer signal can then be modeled with the known parameters, flow, volume, accumulation, dissipation etc [14].

### 2.3.1 Mean and variance of residence time distribution

Important properties from the tracer-response experiment is the mean,  $\bar{t}$ , which will determine the center of the signal at the outlet and the variance,  $\sigma^2$ , that will determine the magnitude of dispersion from the output signal in the detector cell [7]. After running the experiment a certain time, the entire amount of tracer has been detected at the outlet and it can be seen from Figure 2.3 below that the Dirac signal from a pulse injection have dispersed from the initial condition i.e. the concentration variance has increased during the residence time in the vessel. To find the mean of the curve, the sum of the products of concentration at a given time and its corresponding time  $\int_0^\infty tCdt$  is divided by the area under the curve  $\int_0^\infty Cdt$ . The variance is calculated in a similar fashion as seen in Eq. 2.6 [7].

$$\bar{t} = \frac{\int_0^\infty tCdt}{\int_0^\infty Cdt} \quad \sigma^2 = \frac{\int_0^\infty t^2Cdt}{\int_0^\infty Cdt} - \bar{t}^2 \quad (2.6)$$

Using Eq. 2.6 to calculate  $\bar{t}$  for the ideal vessel gives a mean residence time of 1.99 seconds, which is indicated by the Dirac signal in Figure 2.3. This is what the impulse response would look like if there was no dispersion inside the vessel, and clearly this is not the case here. The variance is calculated to  $\pm 1.66$  seconds around the mean residence time ( $\bar{t}$ ). These early peaks before  $\bar{t}$  indicate that specie is transported faster than expected but also that some specie lagging behind after, important indications that will be described further.

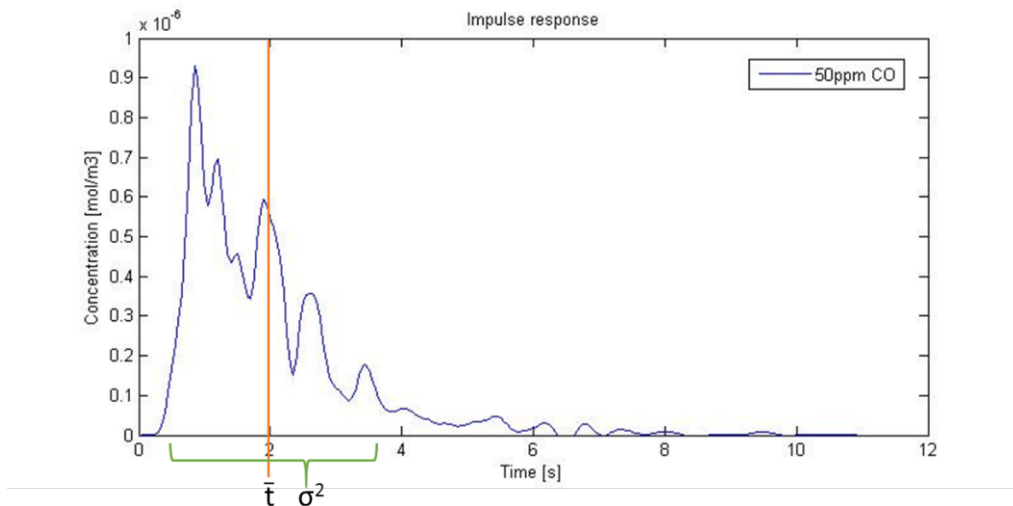


**Figure 2.3:** Mean residence time and variance distribution from a pulse injection.

### 2.3.2 Stagnant zones

If the entire amount of tracer is accounted for, the integral  $\int_0^\infty C dt$  in Eq. 2.6 should be equal to the concentration of tracer at the input. The known tracer input concentration can be compared to the outlet concentration, as they should be equal to fulfill the mass balance (in=out). If not, this is a sign that there are stagnant or dead zones in the vessel that has accumulated tracer specie by diffusion or very slow convection and has therefore remained in the cell or seeping out at very slow rate [7].

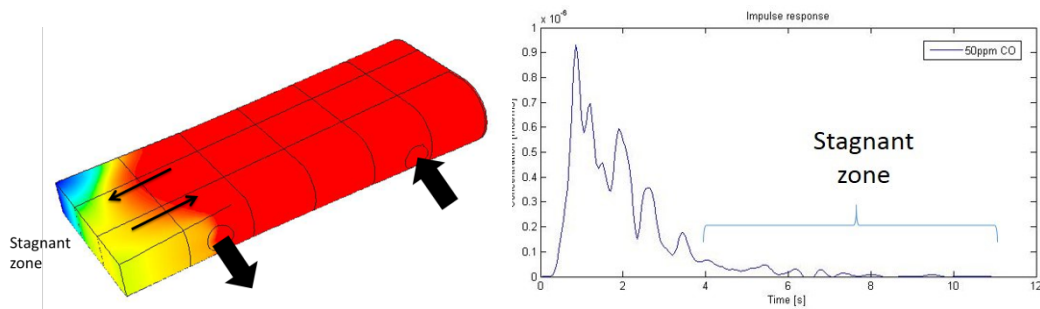


**Figure 2.4:** a) Detector cell with low concentration in stagnant zone. b) Impulse response at the outlet from the detector cell.

Figure 2.4a illustrates a stagnant zone in the cell, and as can be seen the main bulk flow takes the closest route i.e. bypassing to the outlet which leaves part of the vessel stagnant with only tracer transport though very slow convection or diffusion. This will lead to a concentration profile that has a characterized tailing. Seen in Figure 2.4b as a low concentration tailing that eventually will perish. When testing the gas cell with a pulse test off 11.25 sec it can be calculated that there is a small fraction of stagnant zone in the cell. As a rule of thumb [7] the tailing should be cut of at approx.  $3 \times \bar{t}$  and the rest of the tailing is considered to be stagnant fluid.

This means that from 6 sec into the test the outgoing tracer is considered to be contributed by stagnant zone(s).

$$\bar{t} = \frac{\int_{3\bar{t}}^t C dt}{\int_0^{t_f} C dt} \quad (2.7)$$

For our cell this means that a 1.72 % or 3.158 mL of the volume is considered stagnant and looking at the Figure 2.4a above there is a small corner in the cell, which most probably can be considered a stagnant zone. Findings like this is of importance as this small fraction of stagnant volume can be ignored and modeled as regular convective flow as the stagnant volume fraction is so very small. If the volume were to be larger the impact on the model would be considerable.

### 2.3.3 Bypass

Another event that can occur in the vessel is bypassing, the fluid takes the path of least resistance and depending on the geometry of the vessel there can be different routes for the fluid to pass. The bypass is characterized by initial peak(s) of concentration that occur before  $\bar{t}$  [7,15]. This indicates that a partition of the tracer has found a passing that has a faster flow path then the mean bulk fluid. From the concentration profile in Figure 2.3 the high early peaks in the curve is most certainly due to a bypass, and plotting the flow pathways inside the cell shows that there is a flow fraction going directly from inlet following the wall directly to the outlet.

### 2.3.4 Signal conversion

To get as much information and understanding from the experimental data it can be valuable to visually interpret both a pulse-test and a step-response test. Pulse response has the advantage of resolving the events in more detail then the step-response. However the magnitude of the events in a pulse-response can be misleading off the actual impact they pose. This can be seen in Figure 2.5 where the same experiment is presented as both step and impulse response.

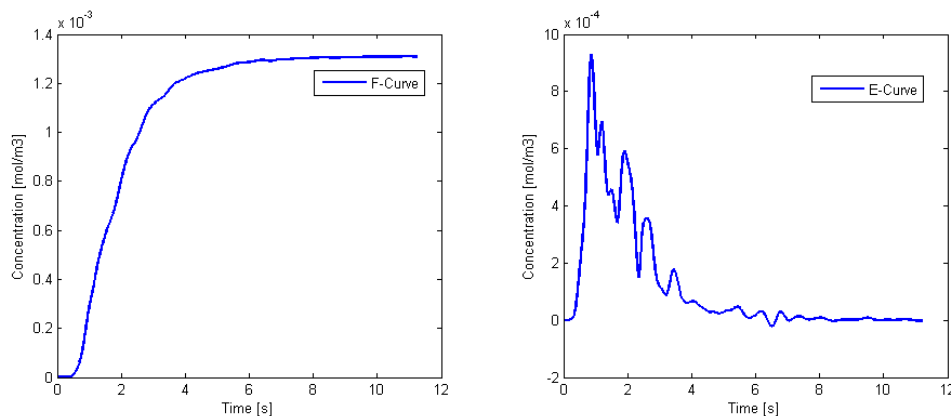


**Figure 2.5:** a) step-response, F-curve. b) Impulse response, E-curve.

The step-response are of equal importance as it presents the concentration front more intuitively for the viewer. Luckily there is no need to do both experiments as they are mathematically related by Eqs. 2.8 and 2.9. Impulse to step response by Eq. 2.8 and rearranged to get the pulse response from the step-response by Eq. 2.9 [7,12,15].

$$E = \frac{dF}{dt} \quad (2.8)$$

$$F = \int_0^t E dt \quad (2.9)$$

## 2.4 Ideal vessels

In order to describe the concentration profile from the detector cell we will formulate a model using the same parameters as the detector cell in the experiment from volume, flow-rate and concentration. As the formulations are theoretical and only contain basic information without accounting for any practical events they are known as ideal vessels. And there are two ideal vessels that can be used to describe the experimental results. The first is a continuous stirred-tank reactor, CSTR, and as the name describes it is a well-mixed vessel that always has a uniform concentration throughout the vessel at any given time. This means as soon the concentration front enters the CSTR, the tracer will be dispersed throughout the vessel and be very diluted. But as the steady input of tracer continues, the concentration of tracer will build up in the vessel until the vessel has the same concentration as the inlet. The second unit is a plug flow reactor, PFR, it will only act as a time delay equal to the mean residence time  $\bar{t}$ , the concentration front going through the vessel will have the exact same concentration profile going out without any distortion [7]. The ideal vessels are illustrated in Figure 2.6 with their corresponding response to an step-input signal.

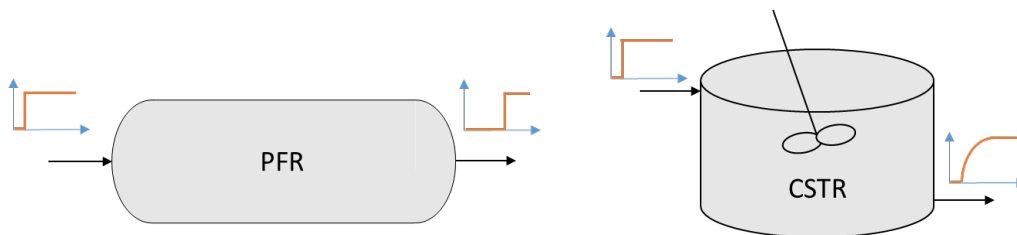


**Figure 2.6:** a) Idealized plug flow reactor. b) and continuous stirred tank reactor.

As evident, using the parameters of cell volume and flow rate for the ideal vessels and comparing them to the experimental result as shown in Figure 2.7, neither of the two idealized vessels show any good comparison and the assumption of idealized flow clearly describe the detector cell poorly. Therefore more in-depth analysis of the detection cell has to be done to allow for a more advanced model to describe the cell behavior, a compartment model.

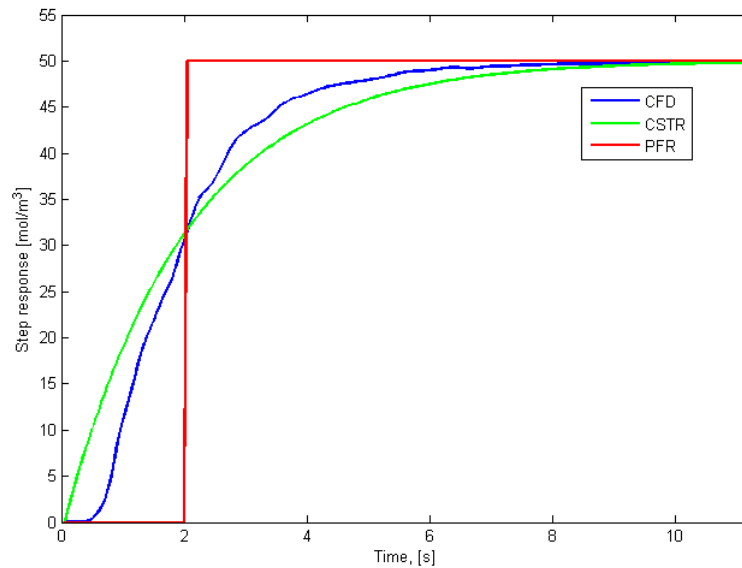


**Figure 2.7:** Comparison between experimental results and idealized vessels.

Understanding the idealized reactors and why these give the result that they do are of importance as they will give an understanding of flow behavior, this insight will be valuable when interpreting the experimental results. Important to say is that ideal reactor vessels are dimensionless and does not contain any spatial information in terms of length, width or height, the vessels only contain volume, and has no known physical shape i.e. the volume of the vessel can have any irregular form [17]. This notion is important later on when the objective is to impose the ir-beam that crosses the vessel with a defined length.

### 2.4.1 Mathematical formulation

In order to simulate the response as shown in Figure 2.7 the formulation had to be translated into a mathematical relationship. This model originate from the general material balance over a control volume which would be our ideal vessel. This complete formulation listed in Eq. 2.10 contains events that can be assumed negligible in the detector cell we want to model [17].

$$\left( \begin{array}{c} \text{Mass flow of} \\ \text{the component} \\ \text{into the system} \end{array} \right) - \left( \begin{array}{c} \text{Mass flow of} \\ \text{the component} \\ \text{out from the system} \end{array} \right) + \left( \begin{array}{c} \text{Rate of} \\ \text{generation/dissipation} \\ \text{of tracer by} \\ \text{chemical reaction} \end{array} \right) = \left( \begin{array}{c} \text{Rate of} \\ \text{accumulation} \\ \text{of mass} \\ \text{in the system} \end{array} \right) \quad (2.10)$$

The CSTR described in Eq. 2.10 can be simplified and still accurately describe the tracer behaviour. Still, it is important to review all the statements in the material balance to review the significance of each term's to the end result. Starting off with the 'Rate in of tracer', this is the inflow of tracer concentration rate  $\frac{mol}{s}$  and it is a product of bulk fluid flow rate ( $\dot{Q} \frac{m^3}{s}$ ) and tracer concentration ( $C \frac{mol}{m^3}$ ). The same applies to rate of tracer out, the ideal CSTR only has one inlet and outlet of CO and will therefore has the same bulk flow rate going out as it has going in. As the

step-response suggest, the concentration of CO (component) will gradually increase from 0 to final concentration, this implies that there will be accumulation of CO. Finally the generation and/or dissipation of tracer by chemical reaction, these are the terms that does not add any significant magnitude to the terms to be included. There is no reaction occurring in the detector cell and is therefore excluded from the material balance. The component balance is therefore simplified [17] and can be rearranged to Eq. 2.11.

$$\left( \begin{array}{c} \textit{Rate of} \\ \textit{accumulation of mass} \\ \textit{of component} \\ \textit{in the system} \end{array} \right) = \left( \begin{array}{c} \textit{Mass flow of} \\ \textit{the component} \\ \textit{into the system} \end{array} \right) - \left( \begin{array}{c} \textit{Mass flow of} \\ \textit{the component} \\ \textit{out from the system} \end{array} \right) \quad (2.11)$$

The following first order differential equation (ODE) Eq. 2.12 is now used to describe the CSTR flow of tracer. This ODE can now be used together with the parameters used in the experiment: volume, volumetric flow and a concentration of tracer to solve for the transient period we want to model [15].

$$V \frac{dC_{out}}{dt} = Q_{in}C_{in} - Q_{out}C_{out} \quad (2.12)$$

# 3

## Methods

At this stage it is obvious that the fluid mechanics of the gas cell cannot be modeled using a single conventional CSTR or PFR, as the gas cell does not exhibit these idealized flow fields predicted by the ideal vessels. Therefore a new approach to the problem is at hand. This is done by viewing the gas vessel as a combination of smaller sections that are interlinked by flow and all these individual sections behaves as ideal reactors (CSTR/PFR) [7,15].

### 3.1 Compartment modeling

The basic modeling units used to puzzle together a compartment model are the CSTR and PFR vessels and the definitions of bypass and stagnant zones. These can be connected in many different ways that yields individual and characteristic concentration profiles. Below in Figure 3.1 are a single CSTR vessel connected with a variety of streams and their resulting RTD are depicted underneath.

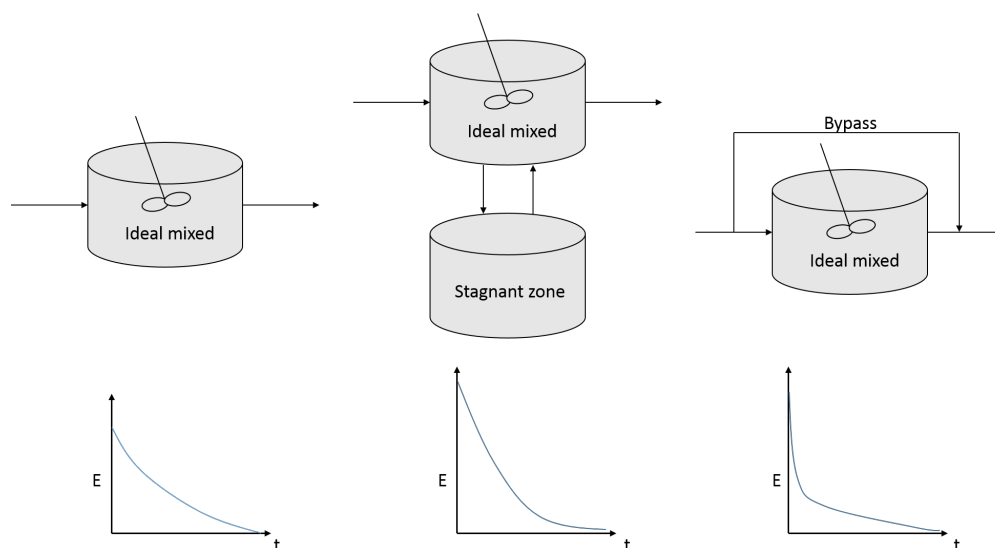


**Figure 3.1:** Different combination of idealized vessels and their outlet response.

Figure 3.1a shows a single CSTR unit with its ideal response. Figure 3.1b shows a CSTR that partially consist of a stagnant zone. This gives a steeper decline in the concentration because it travels more quickly through the part of the CSTR that is active. Figure 3.1c consist of a CSTR but with a bypass, this will lead a part of

the incoming fluid instantaneously to the outlet characterized in the concentration profile as the peak at the start. The rest of the fluid which travels through the CSTR shows the familiar response of the CSTR at a reduced flow-rate caused by the bypass. Which shows as a more flattened decline compared to a standalone CSTR [7].

### 3.1.1 Degrees of freedom

As can be seen from the profiles from the interconnected vessels in Figure 3.1 the resulting concentration profile can be modeled with great flexibility and therefore it should surely not be impossible to puzzle vessels together to get a model almost identical to the experiment. And it is not impossible, but rather labor-intensive as the flexibility in the model increases exponentially as soon as two or more units are connected. For every compartment denoted  $n$  in Eq. 3.1 below, there are a number of parameter freedoms that will have to be set in order to obtain a unique solution. The contribution of parameters for every compartment ( $n$ ) are  $n^2$  number of streams, and  $3n$  is the volumes, initial conditions and final conditions [18].

$$DOF = n^2 + 3n \quad (3.1)$$

This increase in degrees of freedom (DOF) in the model is due to how the total volume should be allocated among the different units and also how the streams should be connected and which streams that are included. Imposing the material balance, the total volume and flow-rate to the streams the compartment model reduces the DOF for a physical compartment model with ‘ $n$ ’ individual compartments by Eq. 3.2.

$$DOF = n^2 + n - 2 \quad (3.2)$$

Eq. 3.2 indicates an exponential growth of parameters as the number of compartments increases, The left scheme in Figure 3.2 below show an example of  $n=2$  for both the unconstrained case and the constrained case.

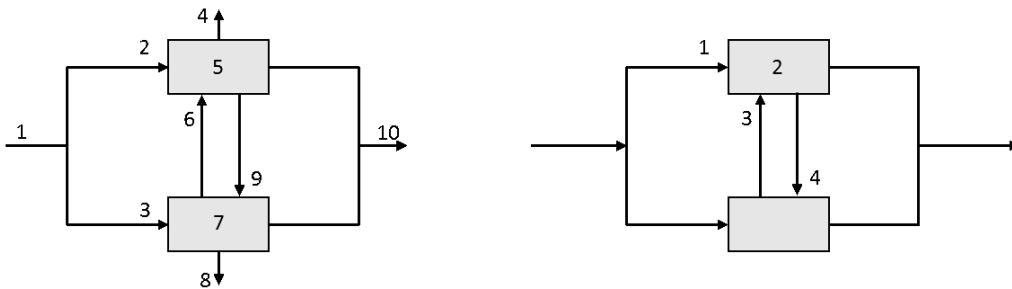


**Figure 3.2:** a) Degrees of freedom in an unconstrained two compartment model. b) Reduced freedoms model based on regular assumptions.

Already here the DOF for two parallel connected CSTR units have numerous ways to split or exclude the flow altogether among the CSTRs, then also how to divide the total volume between the vessels. All of these parameter freedom will have impact on the concentration profile, and adding another reactor unit will increase

the DOF and add complexity. In order to further decrease the DOF there are several assumptions to implement. First of is the assumption that there is no recirculation in the cell, therefore the model is labeled as a ‘trap model’ meaning there is no streams leading back, all the fluid that has entered the system is trapped and can only move forward [18]. The impact of the bypass shown earlier in the experimental data had no significant contribution and could therefore be removed from the model. There is also only a single input and a single output (SISO) from the system, cutting the DOF for each added CSTR by one as it otherwise would have an exit stream for each CSTR unit. Therefore in the end a more bearable number of DOF are left in the end. These parameters concerns the allocation of volume and initial split of flow between the first two parallel CSTR vessels. The DOF in the example above is left with four parameters to model and will be parametrized and fitted by regression analysis.

### 3.1.2 Model condition

In order for the compartment model to predict accurate and reliable results it has to use the same physical properties used in the experiment. The CFD model has used these conditions and are therefore extracted from the software to be used for the compartment model. The conditions of interest from the detector cell are the flow rate and detector cell volume, the spatial information is of no interest as the model is in zero dimensions. The model parameters are set at operating conditions which is defined at atmospheric pressure (101325 Pa) and an elevated temperature at 191°C as the detector cell is heated. These operating parameters are listed in Table 3.1 and can be considered absolute as they will always have to be fulfilled.

**Table 3.1:** Model parameters at operating conditions.

Condition	Value
total volume	183.845 mL
total flow-rate	92.355 mL/s

### 3.1.3 Tanks in series

Before going any further, it can be of interest to see how the response curve (concentration profile) of the compartment model will look by just dividing the cell volume into two or three ideal CSTRs. Illustrated in Figure 3.3 these simple models of two and three tanks in series already represents the experimental data much better than the single CSTR unit.

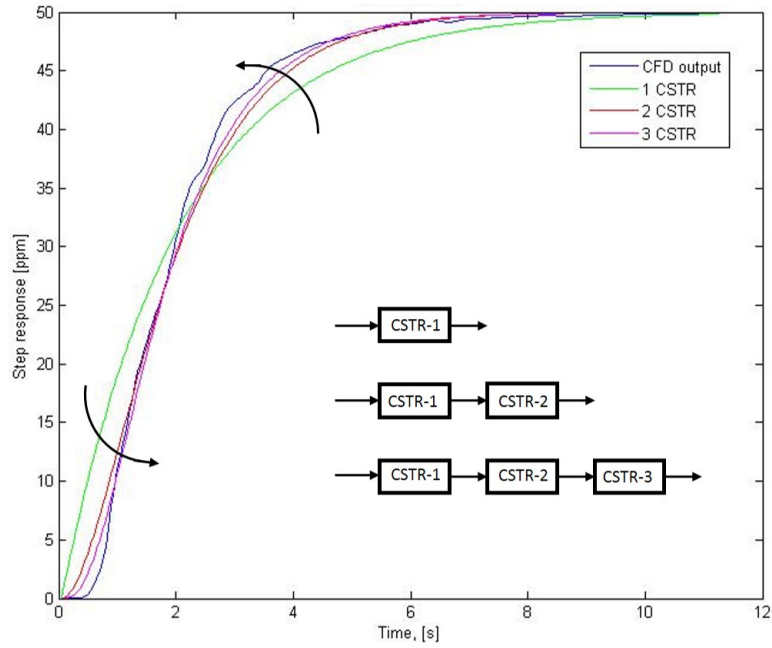


**Figure 3.3:** Tanks in series model fitted towards experimental results.

Figure 3.3 shows how the increasing number of tanks in series converges onto the experimental data. In fact adding on to this series of tanks will slowly move the concentration profile steeper around the pivot point of  $\bar{t}$ . Until you reached a vertical increase when the number of tanks reaches infinity, the same response a PFR would give. This therefore also confirms that a PFR is nothing more than an infinity long tank in series [7]. Therefore if we have need for a PFR as a time-delay we can either model it as the  $f(t-\tau)$  [15] or a long series of CSTR tanks, already at around 100 CSTRs the profile resembles a step response. In the models used in Figure 3.3 the volumes are not equally divided between the CSTR, their volume fraction is optimized to get the highest resemblance towards the experimental data. This optimization is in most regards the core of the compartment modeling and is equally important to optimize as the model architecture itself. The whole process is an iterative procedure where first a model structure is proposed and then the parameters are optimized to the experimental data. The mathematical formulation for these tanks in series will be built up from a system of ODEs and are solved simultaneously and as can be seen from Eqs. 3.3-3.5. The concentration that is derived from the first ODE ( $C_1$ ) cascades down throughout the ODEs, and the final RTD can be monitored by looking at the solution for the ODE containing the output [17].

$$V_1 \frac{dC_1}{dt} = q_0 C_0 - q_1 C_1 \quad (3.3)$$

$$V_2 \frac{dC_2}{dt} = q_1 C_1 - q_2 C_2 \quad (3.4)$$

$$V_3 \frac{dC_3}{dt} = q_2 C_2 - q_3 C_3 \quad (3.5)$$

There should be stated that there is no proof that the tanks in series model actually behaves internally in terms of flow as the actual cell even with a good fit between the experimental data and the model. Therefore the aim is to set out to find a more optimal model for our gas cell. It can be assumed that the flow needs a more complex model than a simple tank in series to predict the internal flow of the detector cell.

## 3.2 Regression analysis

Regression analysis is nothing more than optimizing a mathematical model for describing particular types of pattern in empirical data, and the empirical data would in this case be the concentration profile retrieved from the CFD simulation. Regression analysis is therefore the tool we will use to find the minimal error between the empirical data and our model prediction by having the freedom of changing the volume and flow parameters throughout the compartments model [19]. It is important to know that models never emerge from data, it is we who impose a model on the data and by doing so the model can show changes in the quality of the results from case to case.

*“A model is only a representation designed to display the basic structure of a more complex set of phenomena.”*[20].

For our simplified model this is exactly such a case. A highly complex CFD model that consist of approximately 400000 cells and numerous transport equation of mass, momentum and energy including diffusion that all interact and are solved for three spatial coordinates and time to present the resulting data. The model that are imposed on these data is a much simpler model consisting of 6 cells and one component balance equation without any spatial dimensions except time. It can only be expected that the model only will resolve the basic hydrodynamic dispersion inside the cell [20].

A remark should be made on the modeling structure, there are different ways to attain a model from an empirical data-set. There are of course models that can be fitted to the data without any type of physical relationship, just a purely mathematical construction of polynomials. The possibility to use physical mathematical expressions that are fitted to mimic the flow without any internal structural resemblance to the real flow are also possible, but these two aforementioned models might only show a predictable function for the exact set of data-set used to construct the model against, any changes to the flow which would alter the empirical data-set would not be predictable from the now unreliable models. Figure 3.4 illustrates the flaw in unrealistic modeling as a 7<sup>th</sup> degree polynomial fit can easily and quickly be made with a reasonably good fit within the data-set time-frame. However it is obviate that any predictions further than the 12 sec will be worthless, for this model a small unrealistic/unphysical negative concentration in the very beginning of the experiment will contribute to unrealistic predictions.

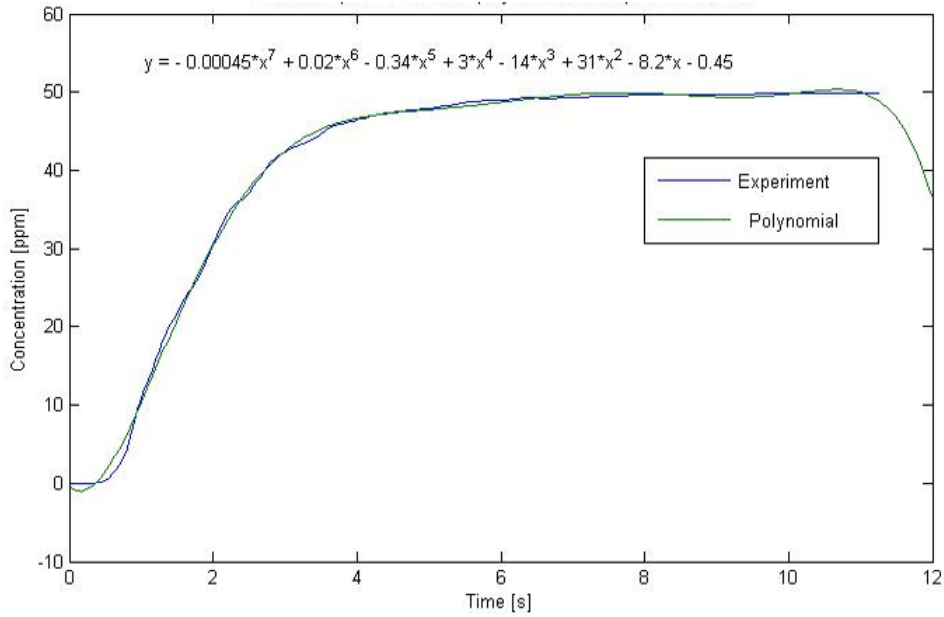


**Figure 3.4:** 7<sup>th</sup> degree polynomial fitted to experimental results.

### 3.2.1 Non-linear regression

To avoid unrealistic models effort have to be made to properly analyze and include relevant terms to assure that the model make physical sense. By investigating the relationship between the dependent (y) and independent (x) variable it is initially established that the regression analysis has to be non-linear for the parameter fitting and will impact the way on how to tackle the regression analysis. The non-linearity comes from the relationship of concentration and flow/volume from the governing CSTR equation. And it is seen by Eqs. 3.6 to 3.9 stating the mathematical relationship analytically.

$$\frac{dC_1}{dt} = \frac{q_1}{v_1}C_0 - \frac{q_1}{v_1}C_1 \quad (3.6)$$

$$\int_0^{C_1} \frac{dC_1}{(C_1 - C_0)} = -\frac{q_1}{v_1} \int_0^t dt \quad (3.7)$$

$$\ln \left( 1 - \frac{C_1}{C_0} \right) = -\frac{q_1}{v_1}t \quad (3.8)$$

$$C_1 = C_0 \left( 1 - e^{-\frac{q_1}{v_1}t} \right) \quad (3.9)$$

From the Eq. 3.9 above the relationship between concentration and flow/volume which is to be parametrized is not linear, it is in fact non-linear as nature tends to be [19]. This is a consequence from the independent variables that will be parametrized in the equation are in a exponential position on Euler's number.

### 3.2.2 Parametrization

The main difference in the final results from linear regression compared to non-linear regression analysis is the approach to find the minimal sum of square error, SSE, between the empirical and model data-set. For the linear regression it can be determined to the absolute or global minimum SSE which comes from that it is a closed data-set and there would be an analytical approach to reach the minimum [19]. The nonlinear regression does not have this analytical approach, instead it uses an iterative procedure. The parametrization for the compartment model uses the ‘trust-region-reflective’ algorithm provided by MATLAB®, which is the default algorithm. This algorithm uses an initial guess and thereafter measures the magnitude of the error derivative, and a new guess is proposed based on the error derivative. This is then repeated until there is no further decrease in the SSE by the minimization algorithm. The internal workings of the algorithm is out of scope for this report and is only mentioned for informational/clarification purpose. By this iterative way of minimizing the SSE there can only be established that a local minimum has been reached. Therefore the quality of the initial guess is very important to make reliable predictions [19].

$$SSE = \sum_{i=1}^n (y_{CFD,i} - y_{model,i})^2 \quad (3.10)$$

For the example earlier with 3 CSTR in series there would be from DOF analysis 10 parameters to specify in order to get a unique solution. This is immediately reduced as we know everything except the individual allocation of the total volume. Therefore there is only two parameters left to be optimized as the third volume will be the remaining volume left from the total volume minus the sum of the other two,  $v_3 = v_{tot} - (v_1 + v_2)$ . The magnitude of the SSE for the three CSTR tank model are dependent on how the two parameters  $v_1$  and  $v_2$  are chosen. Therefore the algorithm will try to minimize the error with respect to  $v_1$  and  $v_2$ , and the following mathematical expression can be derived [24].

$$\frac{dSSE}{dv_1} = 0 \quad (3.11)$$

$$\frac{dSSE}{dv_2} = 0 \quad (3.12)$$

One step after the initial guess these terms will provide a value on how to update the next guess that will minimize the terms until they reach zero and thereby finds an SSE minimum. For a two parameter case this can be visualized by an error surface where you can see the algorithm travel towards the deepest point. From the error surface in Figure 3.5 the solid red line indicate the steps the algorithm takes to reach a minimum.

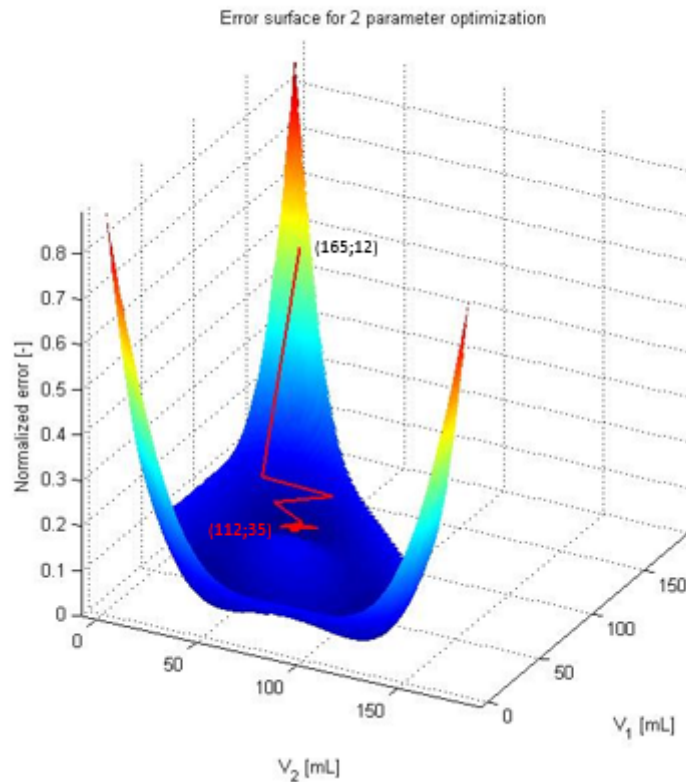


**Figure 3.5:** Normalized error surface for a three tanks in series model.

Depending on the initial guess from the error surface plot in Figure 3.5 there are three possible local minima points visible where the algorithm can travel down to minimize the error. The initial guess was chosen to  $v_1 = 165$  mL and  $v_2 = 12$  mL. Following the red line shows how the algorithm stepped over the error surface until finding the lowest point at one of the three wells. From the surface plot it is clear that we have found one of the three wells that would converge into a minimum error. And without the error plot we would only know that we hit a local minimum. If we try other initial guesses we might end up in another well that has an even lower error sum. The error surface plot is not to be considered a tool which can be used to determine if the best fit has been found or not. The visualization is only possible for one or two parameters as more parameters cannot be visualized in three dimensions. In order to visualize an error surface you need to compute all possible solutions in the boundary range which is highly computationally costly and the error surface here is only to visualize the process of minimizing the SSE.

### 3.2.3 Model structure

To further minimize the SSE between the experimental data and model there is a need to add complexity to the structure to resolve for a more advanced internal flow compared to the simple tank in series model. The new model has a parallel scheme added and internal streams are cross connected to more resemble the internal flow which can be expected in the detector cell. The new compartment model structure

is shown in Figure 3.6 and illustrates the compartment volumes and streams that have to be optimized in order to fit the response profile from the compartment model onto the profile from the CFD model.

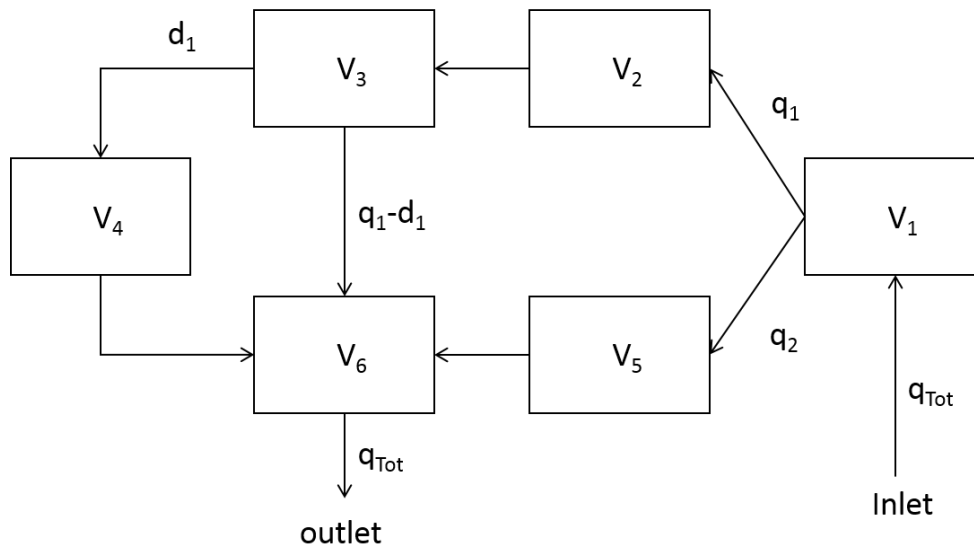


**Figure 3.6:** Compartment model structure with parameters for optimization.

### 3.2.4 Constrained optimization

In the optimizing function there is a need to specify the boundary's for which the parameters should be kept within. The basic outer boundaries are the physical laws that say that there can be no negative volumes, at a minimum they can be zero. We also only have flow in one direction which implies that the flow will only be in a positive direction, and also here a minimum of zero. These will form an outer perimeter on which the parameter will be optimized within and are included in the *lsqnonlin* function as two boundary vectors. For the case where we have reduced a CFD model into 6 compartments the upper and lower boundary constraints can be specified by these physical boundary's.

$$\begin{aligned}
 lb &= \begin{bmatrix} v_1 & v_2 & v_3 & v_4 & v_5 & q_1 & d_1 \\ 0 & 0 & 0 & 0 & 0 & 0 & 0 \end{bmatrix} \\
 ub &= [183.845 \ 183.845 \ 183.845 \ 183.845 \ 92.355 \ 92.355 \ 92.355]
 \end{aligned}$$

As can be seen from the boundary vectors above the last remaining volume and flow parameters are left out. This is due to that these are not parameters that will be optimized. As the DOF analysis showed these last terms are functions of the previous parameters through material balance by Eq. 3.13.

$$v_6 = v_{tot} - \sum_{i=1}^5 v_i \quad q_2 = q_{tot} - q_1 \quad (3.13)$$

All the six individual internal concentration profiles has been included in the penalty function to be optimized. Much of the information can be extracted from the section

CFD model to narrow down the span of what volume each compartment would be. In Eq. 3.14 the sum of squared error, SSE is dependent on the error over the whole simulation time here denoted  $j = 1$  to  $n$   $n = t_f$ . And also for each of the six internal profiles  $i=1$  to 6.

$$SSE = \sum_{i=1}^6 \sum_{j=1}^n (y_{j,CFD} - y_{j,model})_i^2 \quad (3.14)$$

The CFD model provides data from the internal flow which is the best scenario as it will provide the internal flow structure. If however this would not be available the experiment could be performed by two different signals, for example one step response and one sinusoidal signal. Both could be performed in parallel in the objective function and both would be included in the penalty function, illustrated by Figure 3.7 . This would force the parameters to make the best fit of both signals and would increase the chances to fit the compartment model to the internal flow more correctly. However this procedure was not used here as the CFD data provided more detailed information to use.

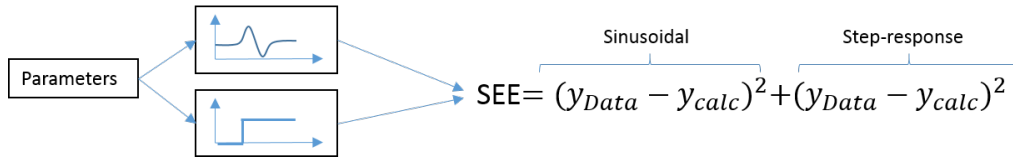


**Figure 3.7:** Introduction of multiple data-set for regression analysis.

### 3.2.5 ODE Solver

There are numerous ODE solvers in MATLAB® that solve ODEs differently. Therefore an analysis of the differential equation is good to optimize the choice of the solver. It has to be taken into account what information we have on the extra conditions. For this mass-balance we have the lower condition for the independent variable,  $C(t)$  at  $t=0$  which is when the cell is empty, therefore  $C(0)=0$ . This calls for an initial-value problem, IVP solver. The compartment model can be exposed to fast changes in the concentration which suggests that the model is stiff. In order to remain accurate and numerically stable, the preferred solver would therefore be an implicit solver that has better stability properties over the explicit solver. From MATLAB® documentation the solver for this problem is the ODE15s solver [24].

### 3.2.6 Script algorithm

Regardless of the layout of the compartment model, from a two series of tanks to a much more complex compartment architecture the same fundamental framework of the MATLAB® script is used to find the optimized parameters. The script has a rather complex structure when it is broken down to the individual components, and therefore a more schematic description of the script is more representative. Starting from the upper left corner in Figure 3.8 all the data that is used are stored in the main script and then transported/sent to the underlying functions, objective functions.

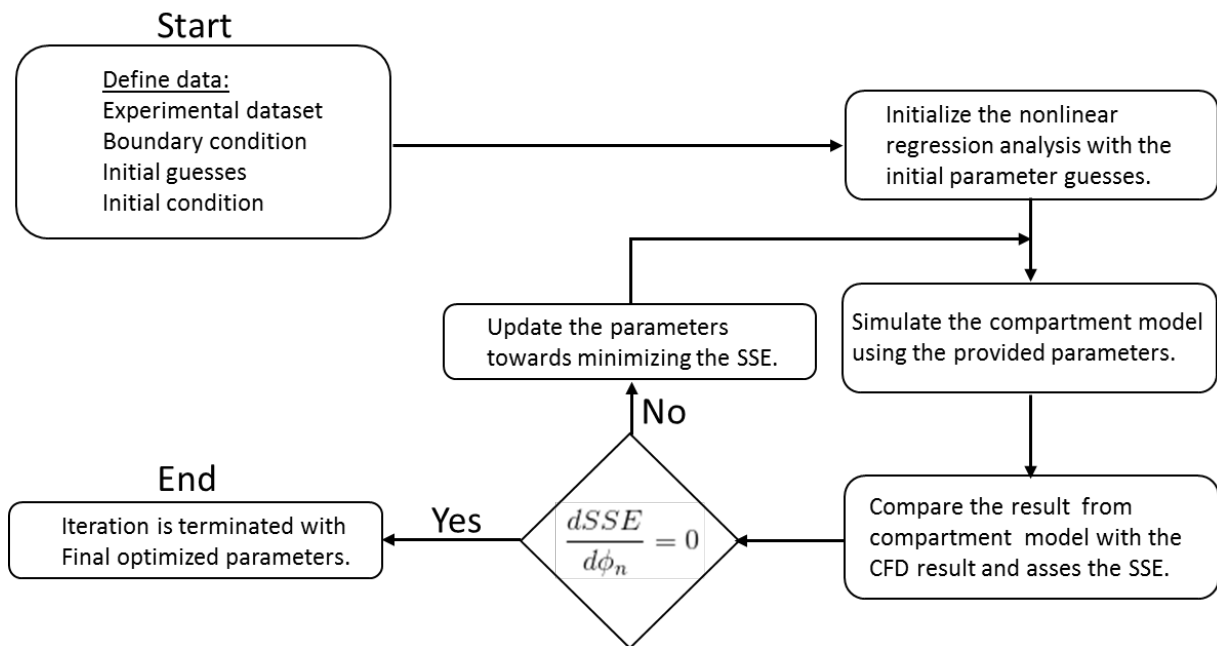


**Figure 3.8:** Procedure for solving nonlinear regression analysis.

### 3.3 Resolving internal flow structure

From earlier sections the focus has been on very simple models as a tanks in series structure to visualize and explain the underlying theory without making the models too complex. These models are however not adequate to model the more complex flow structures inside the detector cell. The algorithm to derive the more complex model structure in order to resolve the internal flow will be reviewed more thoroughly.

#### 3.3.1 Structural design

In order to work out the best mathematical description for the compartment model that fits to the internal flow, the natural step would be to switch the focus from trying to fit the model response to the output (RTD) and instead try to look on how the residence time is actually distributed within the cell. The CFD model of the gas cell was discretized into 18 evenly spaced sections, to be able to monitor the rise of concentration during the transient period which can be seen as an internal RTD for each cell. The individual volumes had also to be extracted from the model as they all varied slightly in size due to that the cell walls vary in curvature as well as the whole cell has a slight wedge geometry. These sections would then have an independently average concentration that would reach the steady state independently from the other sections and will give a sense on how the concentration is spread throughout the cell.

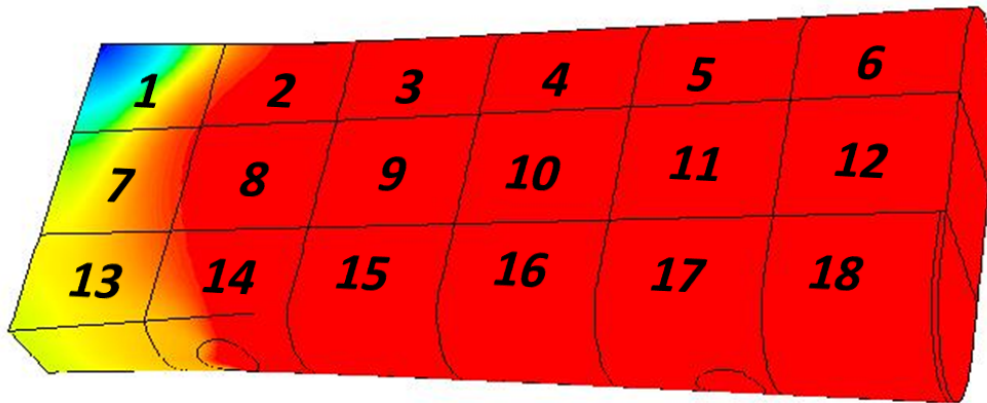


**Figure 3.9:** Discretization of the CFD model into compartments for individual concentration monitoring.

The simulation was run at 50 ppm CO, standard conditions listed in Table 2.1 from the CFD theory section. All the individual sections were monitored until steady-state condition was met. Figure 3.10 below shows the individual sections c-t profiles and the numbers refers to each section. Plotting them together will give a sense of how they interact, as can be seen there are profiles that seems to be similar and are almost intertwined, this gives a clear indication that these sections of volume can be merged together as they overall show similar behavior. This is only true if the profiles follow each other closely during the whole transient period.

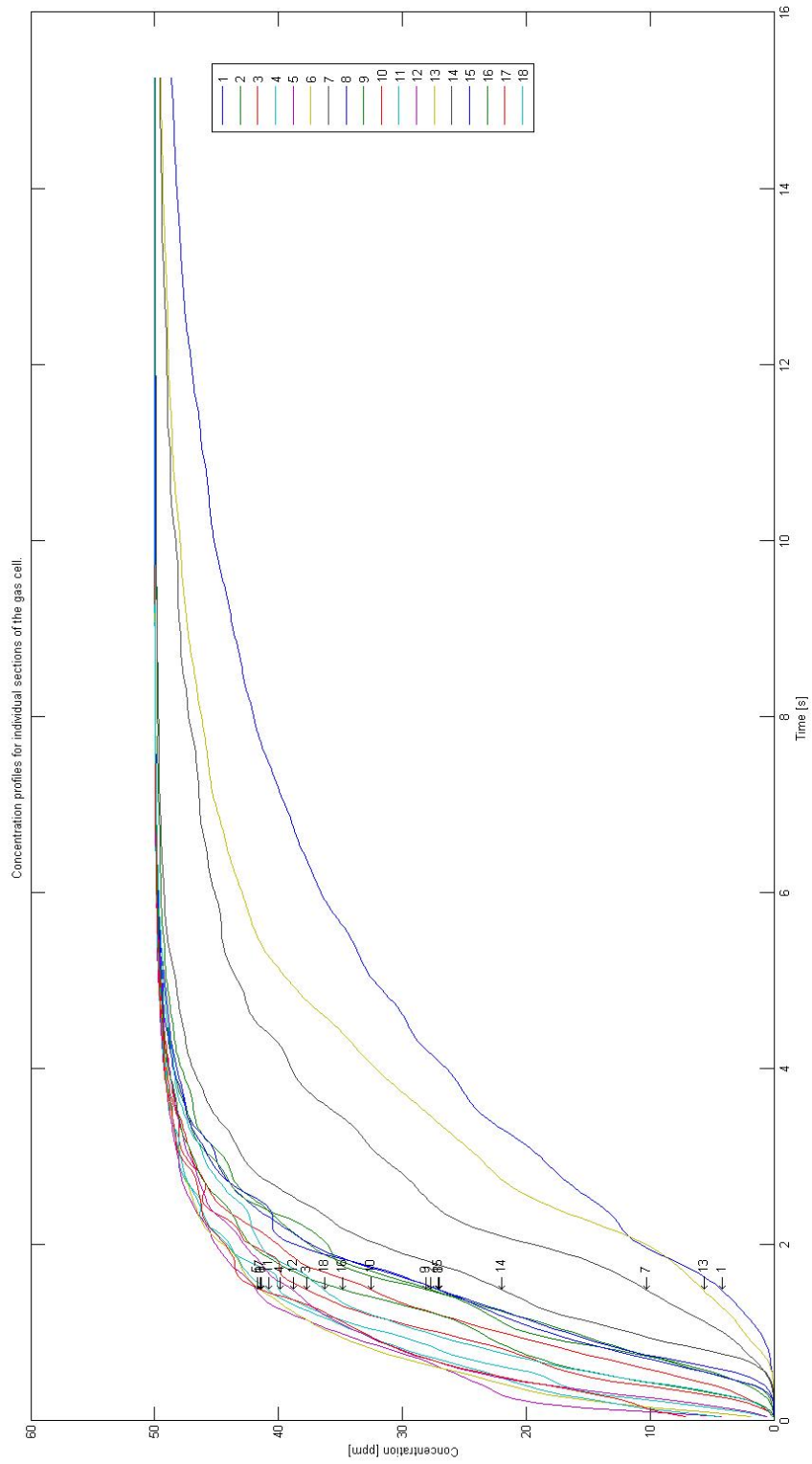


**Figure 3.10:** Individual concentration profiles from the discretized CFD model.

Merging sections that are close together will result in fewer sections that will capture the overall flow pattern and concentration profile throughout the cell. Recorded animations of the internal flow from the CFD simulation which showed the concentration front moving through the cell was used to decide how the streams among the sections should be connected. This work is not a straightforward procedure, and for every section of volume the possibilities of connecting the streams among the compartments starts to branch out as a tree.

The most successful way of performing the procedure and with the best result and fewest possible sidetracks to test, was to first analyze and pair individual sections together, and then one-by-one adding on another section that showed a similar profile. This is where the animation proved most useful to make a more intuitive decision based on how the concentration propagates in the cell. The resulting scheme of how the cell should be discretized in size/volume and sequence/order are shown in Figure 3.11a and the resulting profiles of this scheme is plotted in Figure 3.11b.

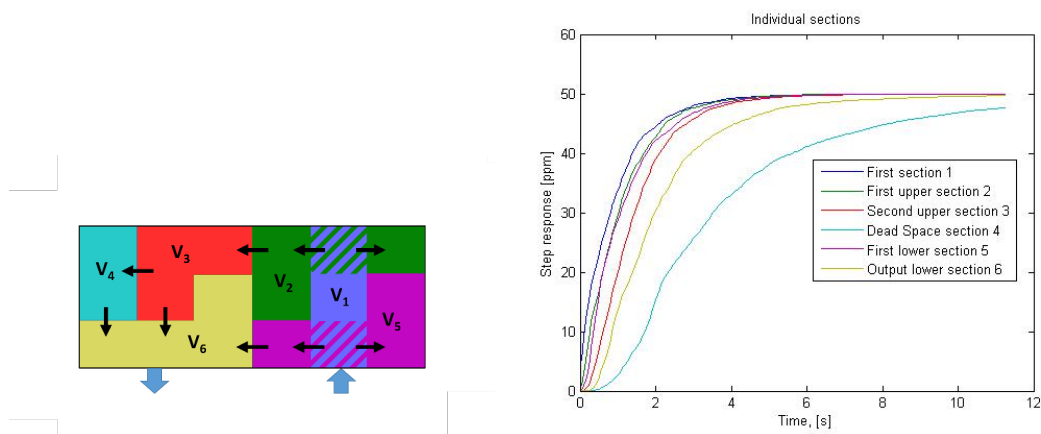


**Figure 3.11:** a) Visualization of the reduced compartments. b) Discretized CFD concentration profiles after cell reduction.

This gives an overall layout that can be used for the compartment modeling. Now the next step is to connect the sections with the significantly most important streams. The most successful way to execute this was to start out with as few connections among the cells as possible to minimize the complexity. Accordingly, the mathematical compartment model was updated in-line with the analysis of the CFD model.

### 3.4 Virtual FTIR

As the original CFD model, the compartment model will be used to compute the FTIR response from the non-homogeneous concentration in the transient period in the cell. And to recapture from the FTIR chapter, due to the nonlinear absorbance spectra from CO the response from the FTIR detector will deviate from what the actual concentration [5]. Therefore the set of equations described in the FTIR section will utilize the transient concentration profiles and volume from each compartment to calculate a concentration based on the Beer-Lambert law, basically the set of

equations will work as a virtual FTIR gas cell. The FTIR equations that are to be implemented are dependent on length which in the zero-dimensional model does not exist. Therefore a weighting factor is used to allocate the total length from the detector used by Bak et al. to derive the non-linear relationship used for the Beer Lambert equation, 6.4 m [5]. The weighting factor used is simply that each volume fractions get an equivalent length fraction depending on the size of the fraction. As put in algebraic expression 3.15 explains.

$$\vec{S}_i = \frac{6.4}{v_{tot}} [v_1 \ v_2 \ v_3 \ v_4 \ v_5 \ v_6] \quad (3.15)$$

The structure how the FTIR response is computed starts off by collecting the optimized volume for each of the six compartments and then allocating a fraction of length to each compartment, as the volumes are static scalars throughout the simulation the same is true for the allocated length, they remain scalar values. The next equation calculates epsilon in each compartment, this is a scalar value for each compartment that is not dependent on the size of the volume in the compartment but only the magnitude of concentration in it. And because the dependent variable is the compartment concentration which is itself dependent on time, the epsilon is therefore also a dynamic variable over time. And for our model the equation will produce six independent epsilon values, one for each compartment. The triplet of epsilon ( $\epsilon$ ), length ( $s$ ) and concentration ( $C$ ) can now be used to calculate an overall absorbance in the cell. Note that the non-linearity has been accounted for by calculating an individual epsilon for each compartment depending on the individual concentration and is now added together, much like the actual detector using the Beer-Lambert law eq 3.16

$$A = \sum_{i=1}^6 S_i C_i \epsilon_i \quad (3.16)$$

The total absorbance (scalar value) is a function of the dependent variable, i.e. concentration, which makes absorbance to be time-dependent. This is of course true as the concentration in the compartment changes over time. The last step is to calculate the concentration detected by the amount of energy absorbed by the previous computations over the compartments. And this is done by making use of the experimentally derived equation from [5] shown in Eq. 3.17.

$$C = -0.981 + 8.781A + 0.554A^2 + 0.00849A^3 - 1.58 \times 10^{-4}A^4 + 7.70 \times 10^{-7}A^5 \quad (3.17)$$

This response can now be compared with the actual concentration in the cell and as shown in Figure 3.12b there is a systematic error from the actual concentration and the calculated FTIR concentration. This is expected, as the same behavior was present in the CFD model seen in Figure 3.12a and is the main purpose to construct the compartment model that can model the deviance that arise from how the actual FTIR handles non-linear absorbance with non-homogeneous concentration distribution.

### 3. Methods

---

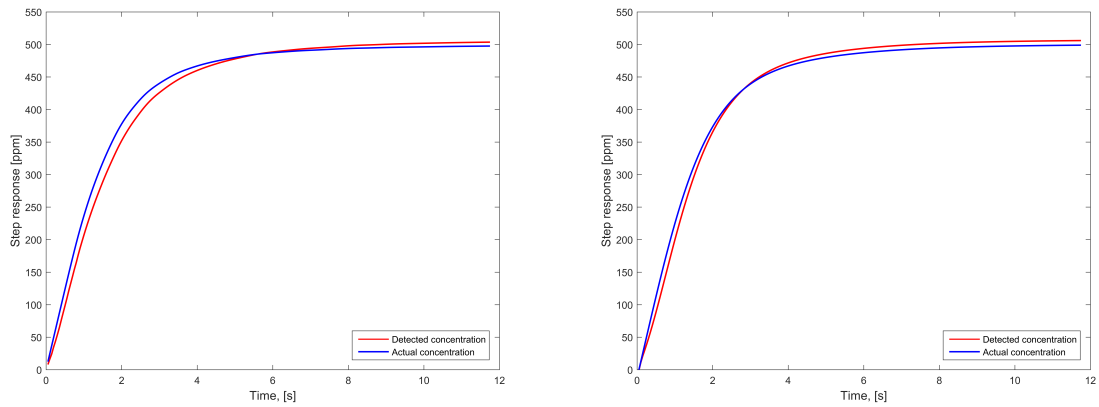


**Figure 3.12:** Systematic error between detected and actual cell concentration for 500 ppm CO in a) CFD model. b) Compartment model.

In order to determine the ability to predict the same systematic error seen in the CFD model, the result from the six cell compartment model is compared to the CFD model that is made up of  $4 \times 10^5$  computational cells. The resulting profiles using identical input for both models is shown in Figure 3.13 and show a good fit between the models.

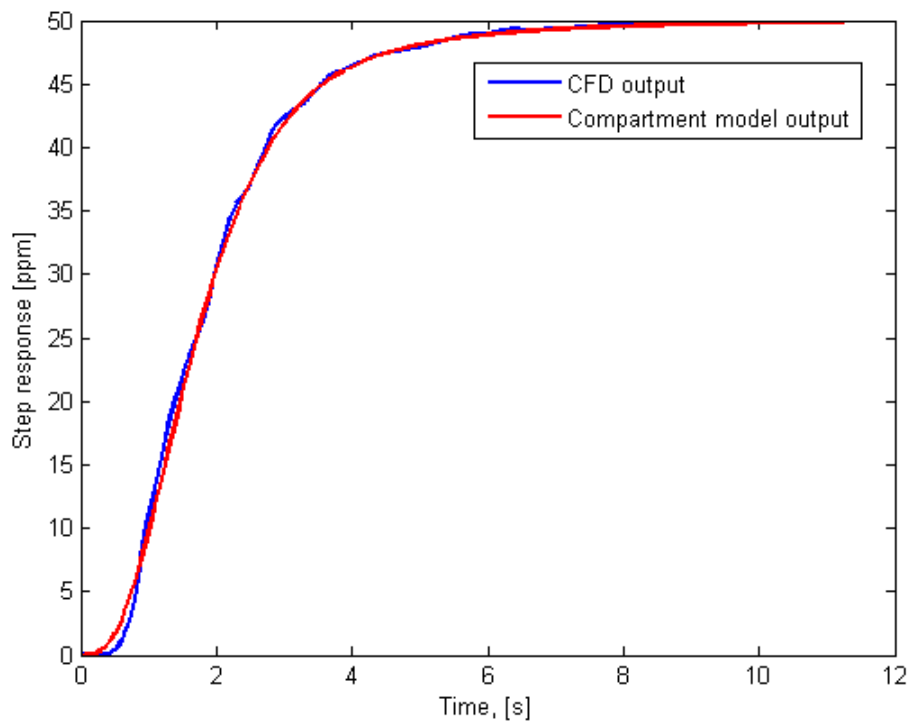


**Figure 3.13:** 50 ppm CO Step response comparison between compartment model and CFD model.

# 4

## Results

There is now a model optimized for the step response of an initially empty compartment to homogeneous steady state of 50 ppm CO at constant flow. For this signal the model predicts well, but the model should preferably be such a good representation of the actual cell that it would do accurate predictions for other types of signals. Therefore the compartment model is tested against new types of signals, flow-rates and concentrations to determine the quality of the model.

### 4.1 Final compartment model

In the beginning it was concluded by analysis of the step response that there was a minimal volume of a stagnant zone of approx. 2 %, and in this model this stagnant zone has been omitted. However the compartment no: 4 is modeled as a compartment that has a reduced convective flow and this has a higher fraction of volume visible as the lagging profile in the Figure 4.1b.

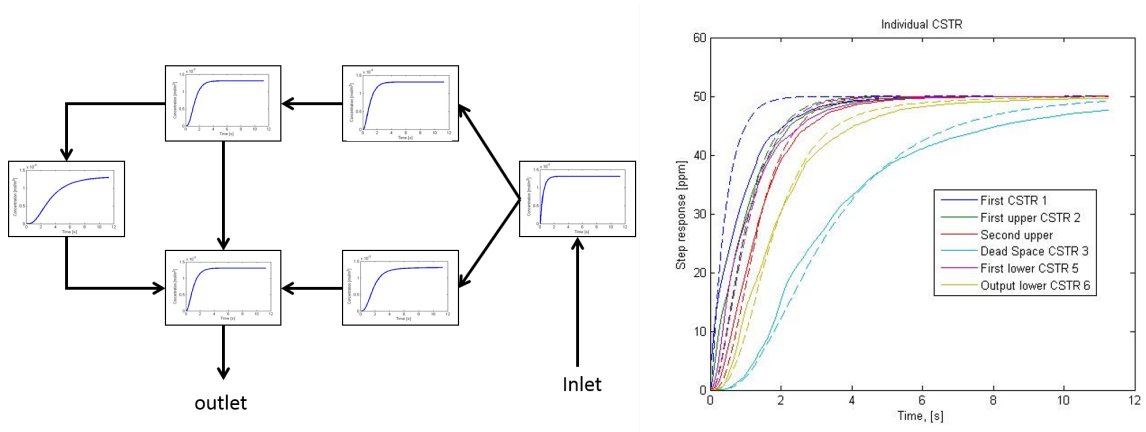


**Figure 4.1:** a) Proposed compartment model with individual step response. b) Comparison between compartment model and CFD results. Solid line CFD profiles, dotted line model profiles.

The compartment model layout that yielded the best resemblance from the optimization to the actual residence time distribution is the scheme in Figure 4.1a. The results between the final compartment model and the sectioned volumes from CFD data can be seen from the plot in Figure 4.1b. Here there is an over estimation in the first CSTR of the compartment model compared to the corresponding section of

the CFD model. However, as will be shown later, this works out by letting the other compartments be slightly underestimated, however the effect on the FTIR response of this error is vanishingly small and is considered acceptable.

**Table 4.1:** Optimal model parameters.

Parameter	Size
$v_1$	38 mL
$v_2$	33.046 mL
$v_3$	17.843 mL
$v_4$	23.758 mL
$v_5$	25.937 mL
$v_6$	45.261 mL
$q_1$	53.432 mL/s
$q_2$	38.923 mL/s
$d_1$	10.105 mL/s

## 4.2 Goodness of fit

When constructing a mathematical model based on a set of parameters in the equations it is valuable to know exactly how much the individual parameters affect each other [20]. Optimally a parameter in the model should not affect another parameter in the model. If it does it can be an indication of poor design or the model is over-parametrized. It can however also be built-in, especially for physical models that are correlated by physical law.

### 4.2.1 Correlation matrix

A first step to investigate the correlation is to look at how two variables change together. The magnitude of covariance between a pair of variables are difficult to interpret, but when divided by the total number of data points, the result will determine the strength of correlation between the variable pair investigated [22].

$$\text{cov}(X, Y) = \sum_{i=1}^N \frac{(x_i - \bar{x})(y_i - \bar{y})}{N} \quad (4.1)$$

The sign of the covariance are more easily interpreted as how the variables are correlated. A negative covariance tells us that an increase in one variable will decrease the other variable or vice versa [23]. All the parameter should be tested against each other and Eq. 4.3 shows the resulting variance matrix for 7 parameters. In the matrix the diagonal is the covariance between the same parameter which will be the

variance as  $cov(p_i, p_i) = var(p_i)$ .

$$\mathbf{V}(\mathbf{p}) = \begin{bmatrix} cov(v_1, v_1) & cov(v_1, v_2) & cov(v_1, v_3) & cov(v_1, v_4) & cov(v_1, v_5) & cov(v_1, q_1) & cov(v_1, d_1) \\ cov(v_2, v_1) & cov(v_2, v_2) & cov(v_2, v_3) & cov(v_2, v_4) & cov(v_2, v_5) & cov(v_2, q_1) & cov(v_2, d_1) \\ cov(v_3, v_1) & cov(v_3, v_2) & cov(v_3, v_3) & cov(v_3, v_4) & cov(v_3, v_5) & cov(v_3, q_1) & cov(v_3, d_1) \\ cov(v_4, v_1) & cov(v_4, v_2) & cov(v_4, v_3) & cov(v_4, v_4) & cov(v_4, v_5) & cov(v_4, q_1) & cov(v_4, d_1) \\ cov(v_5, v_1) & cov(v_5, v_2) & cov(v_5, v_3) & cov(v_5, v_4) & cov(v_5, v_5) & cov(v_5, q_1) & cov(v_5, d_1) \\ cov(q_1, v_1) & cov(q_1, v_2) & cov(q_1, v_3) & cov(q_1, v_4) & cov(q_1, v_5) & cov(q_1, q_1) & cov(q_1, d_1) \\ cov(d_1, v_1) & cov(d_1, v_2) & cov(d_1, v_3) & cov(d_1, v_4) & cov(d_1, v_5) & cov(d_1, q_1) & cov(d_1, d_1) \end{bmatrix} \quad (4.2)$$

The information in the variance matrix ( $\mathbf{V}$ ) is used to normalize the correlation between the parameters with the parameter variance as seen by Eq. 4.3 [24].

$$\mathbf{C}(p_i, p_j) = \frac{cov(p_i, p_j)}{\sqrt{var(p_i)var(p_j)}} \quad (4.3)$$

This will result in a correlation matrix which show the correlation between parameters between the normalized span of -1 to 1. As in the the variance matrix the perfect -1 correlation between two parameters indicate that a positive effect in one will have the exact opposite effect on the other. Indicated by the diagonal a +1 correlation implies that an effect in one parameter will have the exact same effect in the other [23]. Here in the diagonal this is true as the effect is measured between the same parameter. Within the span of -1 to 1 the value will indicate just how strong the correlation are, as a rule, off-diagonal elements does not considered correlation problematic within  $|0.980|$  [19]. The correlation matrix in Eq. 4.4 shows the result of the 7 parameter model with overall very low correlations between parameters which is desirable state.

$$\mathbf{C}_{ij} = \begin{matrix} & v_1 & v_2 & v_3 & v_4 & v_5 & q_1 & d_1 \\ \begin{matrix} v_1 \\ v_2 \\ v_3 \\ v_4 \\ v_5 \\ q_1 \\ d_1 \end{matrix} & \begin{bmatrix} 1.0000 & -0.0411 & -0.0195 & -0.0089 & -0.0458 & -0.0337 & 0.0193 \\ -0.0411 & 1.0000 & 0.9096 & -0.0080 & 0.9513 & -0.4783 & 0.0108 \\ -0.0195 & 0.9096 & 1.0000 & 0.2957 & 0.8002 & -0.6606 & -0.3018 \\ -0.0089 & -0.0080 & 0.2957 & 1.0000 & -0.2185 & -0.6454 & -0.9981 \\ -0.0458 & 0.9513 & 0.8002 & -0.2185 & 1.0000 & -0.1881 & 0.2168 \\ -0.0337 & -0.4783 & -0.6606 & -0.6454 & -0.1881 & 1.0000 & 0.6324 \\ 0.0193 & 0.0108 & -0.3018 & -0.9981 & 0.2168 & 0.6324 & 1.0000 \end{bmatrix} \end{matrix} \quad (4.4)$$

It can be seen from the correlation matrix that the stagnant zone (compartment 4) is highly correlated/dependent on the flow parameter ( $d_1$ ). For compartment 4, a single vessel with a single inlet and identical outlet, with a specified concentration would for any divergence from the specified concentration be penalized. This implies that if you change the volume of the vessel you will have to change the flow-rate to keep the concentration constant to avoid penalty. The effect will be the same for changes in volume were the flow would adjust to keep the concentration constant. This is more evident by looking at the ODE Eq. 4.5.

$$\frac{dC_4}{dt} = \frac{d_1}{v_4} C_3 - \frac{d_1}{v_4} C_4 \quad (4.5)$$

Concentration in compartment 4 ( $C_4$ ) have a profile depending on flow ( $d_1$ ) and volume (V), this profile is fitted to be as similar to the concentration profile from CFD simulation and for every divergence there is a penalty added. The only parameters available for adjustment of  $C_4$  are the flow ( $d_1$ ) entering and leaving the volume (V) which both are embedded in the same term as a fraction. No other parameter has anything to do with these to parameters and they are therefore highly correlated. Therefore the correlation is built-in to the model and the correlation cannot be removed without removing the whole stagnant zone which is highly necessary for the physical flow properties in the model. The resulting mathematical system of linear ODEs are shown here below by Eqs. 4.6 to 4.11.

$$\frac{dC_1}{dt} = \frac{q_1}{v_1}C_0 - \frac{q_1}{v_1}C_1 \quad (4.6)$$

$$\frac{dC_2}{dt} = \frac{q_1}{v_2}C_1 - \frac{q_1}{v_2}C_2 \quad (4.7)$$

$$\frac{dC_3}{dt} = \frac{q_1}{v_3}C_2 - \frac{d_1}{v_3}C_3 - \frac{(q_1 - d_1)}{v_3}C_3 \quad (4.8)$$

$$\frac{dC_4}{dt} = \frac{d_1}{v_4}C_3 - \frac{d_1}{v_4}C_4 \quad (4.9)$$

$$\frac{dC_5}{dt} = \frac{q_2}{v_5}C_1 - \frac{q_2}{v_5}C_5 \quad (4.10)$$

$$\frac{dC_6}{dt} = \frac{(q_1 - d_1)}{v_6}C_3 + \frac{d_1}{v_6}C_4 + \frac{q_2}{v_6}C_5 - \frac{(q_1 + q_2)}{v_6}C_6 \quad (4.11)$$

## 4.2.2 Correlation coefficient

In order to determine the goodness of fit between the final compartment model and the CFD model the output signals are evaluated by the strength of correlation. The magnitude of the correlation coefficient have the same implication as the correlation matrix, the difference lies in that the correlation coefficient will be used to compare the two model functions which results in a scalar value,  $R^2$  instead of all individual variables in the model as the correlation matrix. The output from the compartment model ( $\hat{y}$ ) and the CFD model ( $y$ ) which it was fitted towards is  $R^2 = 0.9994$  and can be considered very strong. The definition is therefore also similar to the correlation matrix which can be seen in Eq. 4.12, where the variable  $\bar{y}$  denotes the mean [24].

$$R^2 = \frac{SS_{Reg}}{SS_{tot,corr}} = \frac{\sum_{i=1}^n (\hat{y}_i - \bar{y})^2}{\sum_{i=1}^n (y_i - \bar{y})^2} \quad (4.12)$$

By dividing the sum of squared residuals  $SS_{Reg}$  with the total sum of squares  $SS_{tot,corr}$  the goodness of fit between the compartment model and the CFD model curve can be assessed by the resulting correlation coefficient  $R^2$ , the result shown below indicates a very good fit, partly in this case as the compartment model is specifically fitted towards the CFD model.

$$R^2 = 0.99945 \quad (4.13)$$

### 4.3 Concentration

Changes in the magnitude of concentration in the step-response from the compartment model and CFD model will result in the exact same concentration profile (RTD), the only change is in the concentration magnitude and thus not change any of the flow properties [3]. Increase in the inlet concentration does not alter the flow structure by the optimized parameters. The concentration profile will therefore remain constant when changing the magnitude of concentration at inlet as indicated by Figure 4.2. The fixed profile is due to the specie transport through the detector cell remain constant regardless the concentration as the concentration magnitude does not affect the RTD.

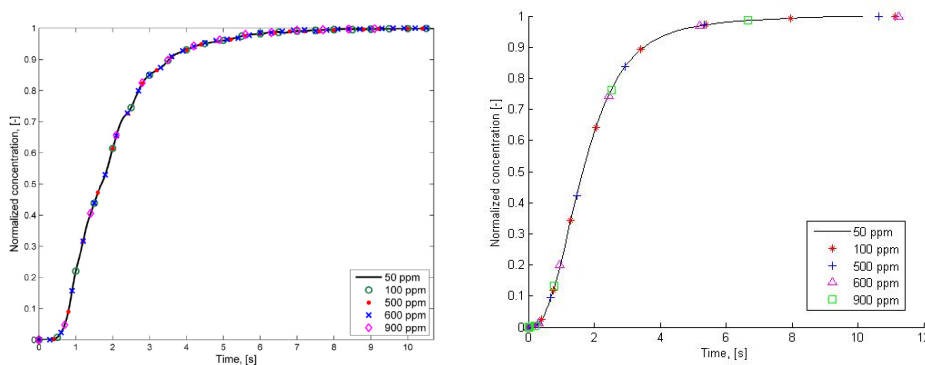


**Figure 4.2:** Step-response for 50,100,500,600 and 900 ppm CO concentrations simulated by (Left) CFD, (Right) compartment model.

## 4.4 Variance

Throughout the transient period of both CFD and the compartment model there is a non-homogeneous concentration in the cell. The magnitude of this variance will indicate a degree of non-homogeneity. Figure 4.3 compares the results from the compartment model and CFD simulations. The most striking difference between the two are the lower variance after they both have reached their peak. This is most probably due to that the compartment model overestimates the degree of mixing in the cell. However the impact on this difference in variance will be shown to have little effect on the model quality, as shown later in this chapter.

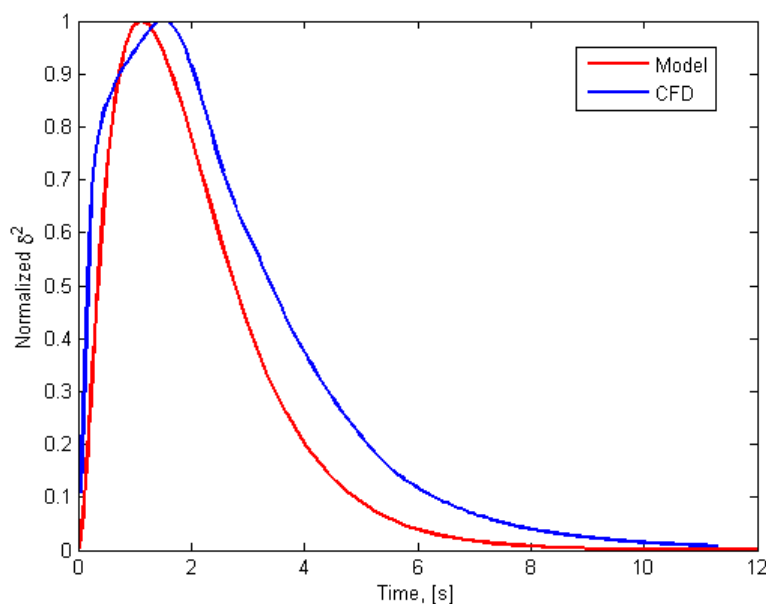


**Figure 4.3:** Comparison of variance from a step response between CFD model and compartment model at 50 ppm CO.

## 4.5 Sinusoidal signal

The model ability to predict the response from a sinusoidal test signal was evaluated for a simulated flow time of 27 seconds in a transient simulation with the same properties as before, but with a sinusoidal frequency  $1\text{rad/s}$  ( $1\text{rad/s} = 1/2\pi\text{Hz}$ ). The signal alternated between zero and 500 ppm of CO and from Figure 4.4 it is observed that the model correlates to the CFD model fairly well. While CFD simulation which took approximately 96 h to compute, the compartment model took only 0.08 s. It is also shown in the graph that the concentration actually never reaches the set point, i.e. 500 ppm. This is due to the fast changes in the sinusoidal signal which the overall cell concentration cannot keep up with.

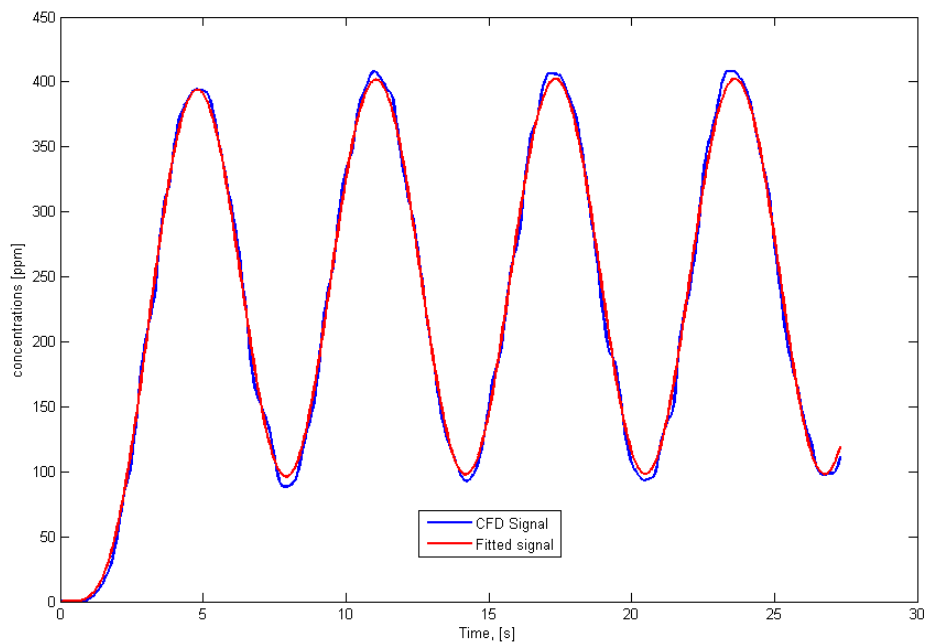


**Figure 4.4:** Comparison between CFD and compartment model of a 27.3 sec Sinusoidal test signal.

An extra remark should be made that the compartment model is fitted from a 11.3 sec long data-set, and is in the test above able to predict a response with high accuracy that was almost 3 times as long. The accuracy for this test signal is still high with a correlation coefficient between the sinusoidal data-set and model at  $R^2 = 0.9990$ .

## 4.6 Variable flow-rates

The credibility of model accuracy regarding the prediction of concentration profile is strong and the focus is therefore shifted from the concentration variable to the flow. The aim is to investigate if the model can be used at other flow-rates than it was fitted for and still remain accurate. The CFD model was simulated with -60 %, 50 % and 60 % of the nominal flow-rate of 92.355 mL/s at 191°C and 1 atm. The result still shows a good match which is confirmed by Figure 4.5, solid lines represent the CFD response, and the dashed lines are the model response.

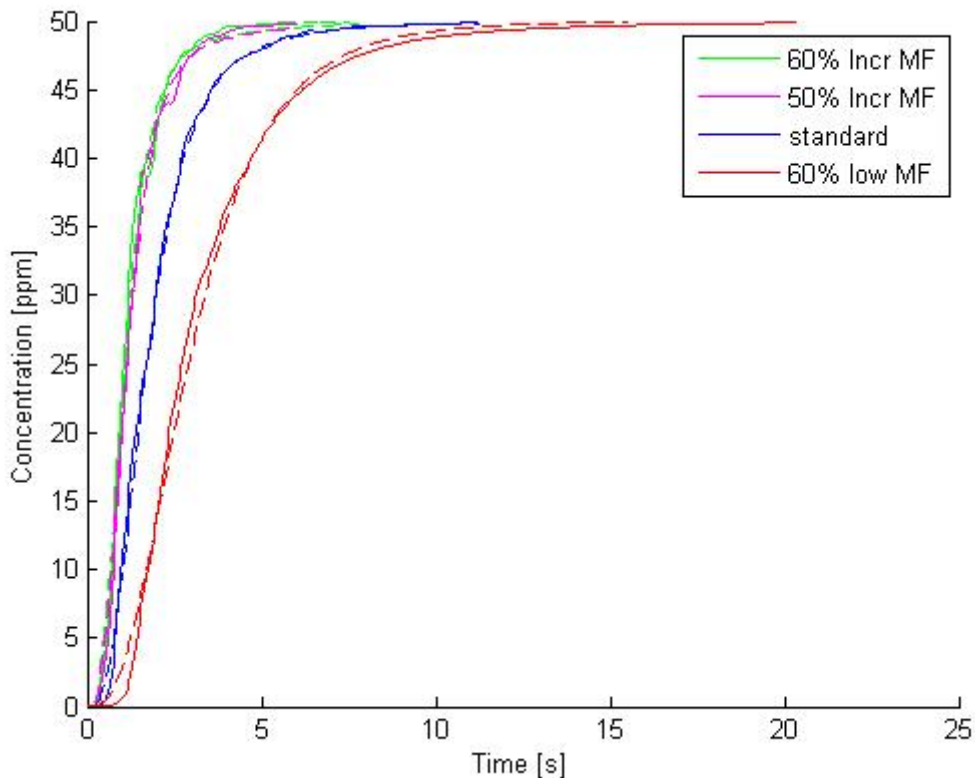


**Figure 4.5:** Comparison between CFD and compartment model at -60%, std., 50% and 60 % the nominal (92.355 mL/s) mass flow-rate.

The correlation coefficients from the variable flow-rates are  $R_{-60\%}^2 = 0.9986$ ,  $R_{+50\%}^2 = 0.9988$  and  $R_{+60\%}^2 = 0.9982$ . The model therefore show to make accurate predictions reasonably well in this -60 % to 60 % flow variation. It is therefore possible to add a dynamic flow variable to the model (assuming the flow rate of the gas mix in the experiment fluctuates within  $\pm 60$  %).

## 4.7 FTIR comparison

As the internal flow has been thoroughly tested and evaluated, the final test is now to compare the detected concentration profile from the implemented non-linear absorbance relationship. The resemblance in the predicted result from the virtual FTIR detected response is the main objective and as Figure 4.6 shows for the case of 500 ppm CO the fit between the models are accurate and shows that the compartment model can accurately predict and account for the systematic error.

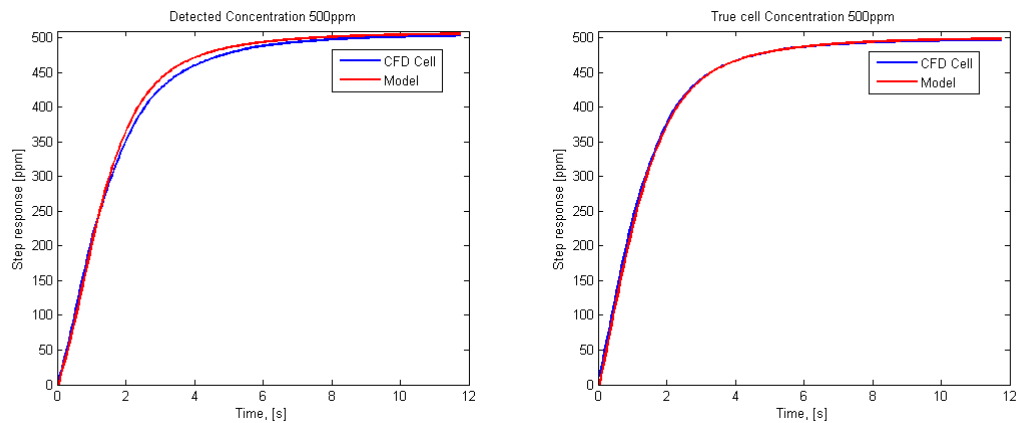


**Figure 4.6:** Detected concentration by the CFD and compartment model at 500 ppm.

## 4.8 Computational time

An important aspect of the compartment model is how well it reduces the computational power compared to the CFD model. The CFD model requires a large amount of computational power and time to compute useful data. The compartment model on the other hand does not require any substantial computational power and the computational time is in the span of a 23 millionth of what the CFD uses. For comparison the computer specification together with the computational time is listed in the Table 4.2.

**Table 4.2:** Computer and software specifications.

TYPE:	CPU	RAM	MODEL	TIME	OS	SOFTWARE	SIZE
MODEL	2.6 GHz	8GB	Laptop	0.05 sec	Win 8	MATLAB R2013b	1KB
CFD	3.1 GHz	16GB	Desktop	96 h	Win 7	Ansys Fluent R15.0	166MB

A series of simulation with varying simulation length was performed to look at the increase in computational time. The signal used for this simulation was the sinusoidal test signal with an amplitude between zero and 500 ppm CO, and each simulated second contained 20 data points. The results determined a linear relationship with simulated time and the time it took to compute the resulting simulation. This makes it easy to predict the computational time for longer simulations. And the still very low computational times makes the model highly useful to incorporate in an iterative algorithm where it can be used repeatedly tenths of thousands of times without adding any substantial time to the simulation.



# 5

## Conclusion

Using the CFD model as a basis to develop the compartment model was shown to be an excellent source in the sense of the ability to extract information about flow, concentration and dynamic behaviour. The quality of the proposed framework for the compartment model was tested by changing the main operating condition of flow-rate, concentration and the profile of the ingoing signal. All results were compared by statistical methods. The high correlation coefficient for the final compartment model  $R^2 = 0.99945$  shows great potential for the model to predict the segregation inside the FTIR cell. Additional tests confirm the model allows prediction with high accuracy also at conditions different from the one used in the regression analysis. The compartment model was able to reduce the computational time for an 11 sec simulated sequence from 96 h to 0.05 sec on a standard desktop computer. This reduction in computational demand was a important criteria to fulfill, and enables the model to be incorporated in non-linear regression analysis.

These initial results produced by the compartment model indicates that the model will provide reliable data as a corrective algorithm when resolving the transient kinetic information and as result, provide higher quality in the parametrization and understanding of transient kinetics supplied by the experimental data.



# 6

## References

1. Johnson KA. The Enzymes. Pennsylvania, Elsevier, 1992. p. 1–61.
2. Soltani S, Wang-Hansen C, Andersson R, Andersson B. CFD characterization of monolithic reactors for kinetic studies. *Can J Chem Eng.* 2014,92(9):1570–8.
3. Soltani S, Andersson R, Andersson B. Time resolution in transient kinetics. Springer 2012,592.
4. Soltani S, Andersson R, Andersson B. Enhancement of time resolution in transient kinetics. *Chem Eng J.* 2015,264:188–96.
5. Bak J. Quantitative Gas Analysis with FT-IR: A Method for CO calibration using partial least-squares with linearized data. *Appl. Spectrosc.* 2001,49(4):437–43.
6. Berthomieu C, Hienerwadel R. Fourier transform infrared (FTIR) spectroscopy. *Photosynth Res.* 2009,101(2-3):157–70.
7. Levenspiel O. Tracer technology modeling the flow of fluids. R M, Madylam, editors. Springer, 2012. p.153
8. Larkin P. Basic Principles. In: *Infrared and Raman Spectroscopy, Principles and Spectral Interpretation and Raman Spectroscopy.* Elsevier 2011. p. 7–25.
9. Haaland D. Methods to Include Beer's Law Nonlinearities in Quantitative Spectral Analysis. In: *Computerized Quantitative Infrared Analysis.* 1987. p. 1–8.
10. MKS Instruments I. FTIR Gas Analysis. Andover, MA: MKS Instruments, Inc, 2007. p. 1.
11. J.Kestin, Ro ST, Wakeham WA. Viscosity of the noble gases in temperature range 25-700°C. *J Chem Phys. J. Chem. Phys,* 1971,56(8):4122.
12. Schobeiri MT. *Applied Fluid Mechanics for Engineers.* McGraw-Hill, 2014. chp 8 p.
13. Andersson B, Håkansson L, Andersson R, Mortensen M, Sudiyo R, Van Wachem B. *Computational fluid dynamics for engineers.* Cambridge University Press, Cambridge 2011. 24-61 p.

14. Levenspiel O. Chemical reaction engineering. 3rd ed. Wiley, 1999.
15. Fogler HS. Elements of chemical reaction engineering. 4th ed. Prentice Hall, 1999.
16. Bera RK, Bandyopadhyay, A.K., Ray PC. Mathematical Physics for Engineers. In: Mathematical Physics for Engineers. Kent: Academic Science, 2015. p. 25–8.
17. Ingham J, Dunn IJ, Heinzle E, Prenosil JE, Snape JB. Chemical Engineering Dynamics. 3rd ed. Weinheim, 2007. p. 1-20
18. C. Y W, L.T F. Models for flow systems and chemical reactors. Lyle F. A, R.N. M, John J M, editors. New York: Marcel Dekker, 1975. p. 251-277
19. James F. Rusling, Kumosinski. TF. Nonlinear computer modeling of chemical and biochemical data. Academic Press, 1996. p. 268
20. Allen MP. The origins and uses of regression analysis. Understanding Regression Analysis. Washington: Plenum Press, 1997. p. 1-5
21. Åström KJ, Murray RM. State feedback. In: Feedback systems: an introduction for scientists and engineers. Princeton University Press, 1995. p. 169–71.
22. Mukhopadhyay, Nitis. Correlation Coefficient, International Encyclopedia of Statistical Science. Springer Berlin Heidelberg. 2011, p. 315-318.
23. Morrison J. Statistics for engineers, Hoboken, Wiley, 2015. p. 9 – 30.
24. Rasmuson, A., Andersson, B., Olsson, L. & Andersson, R. , Mathematical modeling in chemical engineering, Cambridge University Press, Cambridge, 2014
25. Levenspiel, Octave, Tracer technology: modeling the flow of fluids, Springer, New York, 2012

# A

## Appendix 1

### A.1 Investigation of time invariance in CFD model

The system is assumed to be time invariant, meaning that it does not matter at which time the signal is put on the system. Therefore a series of time delays was simulated and compared to be matched with each other. The series of simulations was implemented by delaying the start of the step response at the simulation start. i.e. the simulation started at  $t = 0$  but the step response signal was not implemented onto the system until a certain delay had past. All the other parameters on the simulations remained equal to each other except these time delays of 0.3, 0.4, 0.5, 0.6, 0.7 seconds. In a time invariant system the concentration profiles keep identical to each other only spaced out on the time axis due to the delay. The Figure A.1 below the delays has been removed to superimpose the profiles to easily visualize any divergences.

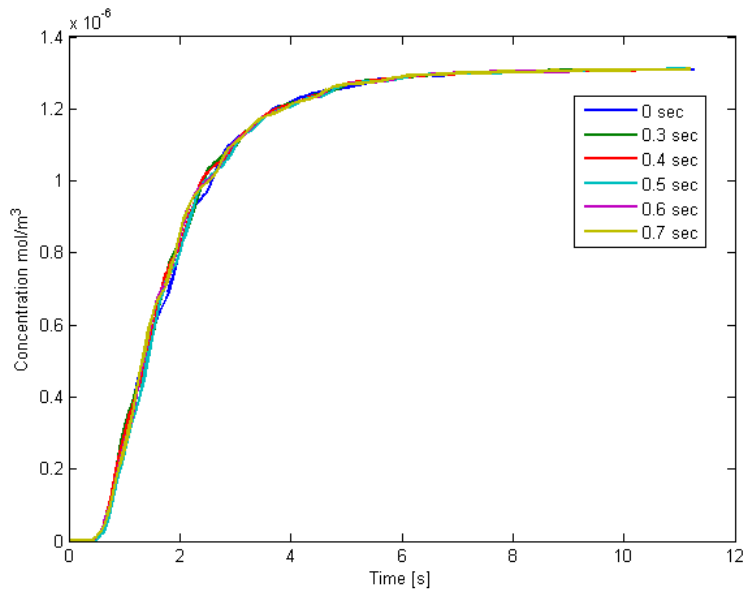


**Figure A.1:** Comparison between CFD simulated time delays with normalized starting point at  $t = 0$ .

As the picture shows there are no larger deviations but still they are not exactly equal which implies that the system in fact is not time independent, it makes a difference when the signal or experiment starts. By comparing the error between

the profile without delay to all individual profiles with delay there cannot be seen a pattern that can be converted to a cyclic mathematical function that can be imposed onto the compartment model as Figure A.2 below shows.

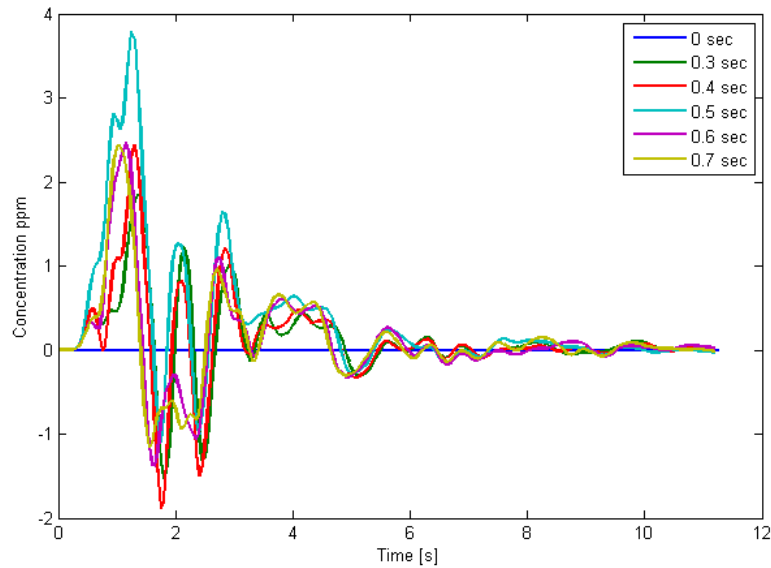


**Figure A.2:** Error between no delay and 0.3, 0.4, 0.5, 0.6 and 0.7 sec time delay.

The cause for this time variant behavior is assumed to be due to the convective flow at the inlet that forms as jet. On transient animation this jet has shown to have a cyclic motion that swirls around the inlet axis. This motion seems to be fairly chaotic and does not follow any obvious pattern that can be predicted with any high precision to incorporate it in the compartment model. However the magnitudes of the differences are relatively small and the assumption will therefore be that the system still is time invariant.